Chemical Science

ROYAL SOCIETY OF CHEMISTRY

PERSPECTIVE

View Article Online
View Journal | View Issue

Cite this: *Chem. Sci.*, 2025, **16**, 6542

All publication charges for this article have been paid for by the Royal Society of Chemistry

Glutathione: a naturally occurring tripeptide for functional metal nanomaterials

Zhucheng Yang, [ab] Jingkuan Lyu,[ab] Jing Qian,[ab] Yifan Wang, [ab] Zhenghan Liu,[ab] Qiaofeng Yao, [ef] Tiankai Chen, [*c] Yitao Cao*[d] and Jianping Xie [*ab]

Glutathione (GSH), a naturally occurring tripeptide, plays an important role as an intracellular antioxidant in the physiological microenvironment and participates in redox balance, detoxification, and cellular and disease regulation. The unique structural features of GSH, including the reductive thiol and multiple coordination sites (carboxyl and amino group), make it a significant molecule not only in the physiological context but also as a ligand in the development of functional metal nanomaterials. In this context, GSH's role as a protective ligand and reducing agent in surface etching and ligand exchange reactions has been explored at the molecular level, expanding the diversity of GSH-protected metal nanomaterials. With photoluminescence (PL) as one of its most intriguing properties, investigations into GSH's influence on PL properties emphasize its multifaceted coordination capabilities in surface coating, charge transfer from electron-rich functional groups, chirality arising from its unique structure, and available conjugation sites. Moreover, the biocompatibility of GSH, combined with the synergistic effect of metal components, renders GSH-protected nanomaterials an "Inseparable Duo" highly suited for applications in bio-sensing, bio-imaging *via* PL radiative decay and anti-cancer bio-therapies through photothermal therapy, photodynamic therapy, and radiotherapy. By exploring the multifaceted roles of GSH, this *Perspective* aims to highlight pathways including the encouragement of deeper synthetic exploration, innovative design at the bio–nano interface, and expanded nanobiomedical applications.

Received 20th December 2024
Accepted 8th March 2025

DOI: 10.1039/d4sc08599j

rsc.li/chemical-science

[a]*Joint School of National University of Singapore and Tianjin University, International Campus of Tianjin University, Fuzhou 350207, P. R. China*

[b]*Department of Chemical and Biomolecular Engineering, National University of Singapore, Singapore 117585, Singapore. E-mail: chexiej@nus.edu.sg*

[c]*School of Science and Engineering, The Chinese University of Hong Kong (Shenzhen), Shenzhen 518172, P. R. China. E-mail: chentiankai@cuhk.edu.cn*

[d]*National and Local Joint Engineering Research Center of MPTES in High Energy and Safety LIBs, Engineering Research Center of MTEES (Ministry of Education), Key Lab. of ETESPG (GHEI), South China Normal University, Guangzhou 510006, P. R. China. E-mail: cao_yitao@m.scnu.edu.cn*

[e]*Key Laboratory of Organic Integrated Circuits, Ministry of Education, Tianjin Key Laboratory of Molecular Optoelectronic Sciences, Department of Chemistry, School of Science, Tianjin University, Tianjin 300072, P. R. China*

[f]*Collaborative Innovation Center of Chemical Science and Engineering (Tianjin), Tianjin 300072, P. R. China*

Zhucheng Yang

Zhucheng Yang received his BS degree (2020) from the University of Chinese Academy of Sciences. He is currently pursuing his PhD degree under the supervision of Prof. Jianping Xie at the National University of Singapore. He is now interested in the smart synthesis and ligand-driven programming of metal nanoclusters.

Jingkuan Lyu

Jingkuan Lyu is a PhD student at the National University of Singapore under the supervision of Prof. Jianping Xie. He obtained his BS degree in chemical engineering from the same university. His research interest focuses on the automated synthesis of gold nanoclusters, integrating in situ and real-time characterization, robotic synthesis and machine learning.

1. Introduction

Glutathione (denoted as GSH or SG) was initially isolated in 1888 by De-Rey-Pailhade, who named the substance "phylothion", derived from Greek for sulfur-loving. Subsequently, in 1921, Frederick Gowland Hopkins elucidated its structure, identifying it as a tripeptide consisting of glutamine, cysteine, and glycine.[1,2] This structure is characterized by a distinctive γ-glutamyl linkage that joins the glutamine and cysteine residues. Its unique chemical structure decides the fundamentals of the physiological roles of GSH.[3] For instance, the distinct γ-type peptide bond in GSH confers resistance to hydrolysis by peptidases, while the glutamate residue protects it from degradation by γ-glutamyl cyclotransferase.[4] These features endow GSH with enhanced stability throughout metabolic processes. Additionally, the presence of various functional groups in GSH, including carboxyl (–COOH) and amino ($–NH_2$) groups, grants it exceptional metal coordination abilities, facilitating *in vivo* detoxification processes. Crucially, the free thiol group (–SH) in GSH is highly reactive and can be easily oxidized to form glutathione disulfide (GSSG), a property that underpins GSH as a vital antioxidant in numerous physiological processes.[5] As a result, GSH has emerged as one of the most essential and extensively investigated molecules in the fields of biochemistry and cell biology.[6–9]

The physiological significance of GSH has been further clarified over the years, highlighting its participation in numerous biological processes (Fig. 1). Its most notable function is in regulating the redox balance within cells, a critical mechanism for preventing cellular damage induced by reactive oxygen species (ROS).[10,11] ROS are metabolic byproducts that, if not properly managed, can induce oxidative stress, leading to damage to DNA, proteins, and lipids. GSH mitigates ROS through its redox cycle, wherein GSH is oxidized and subsequently reduced by GSH reductase, thereby maintaining a sustained availability of this critical antioxidant within the cell.[12] Beyond its

Jing Qian

Jing Qian obtained his BS (2021) from the National University of Singapore. He is currently a PhD student under the supervision of Prof. Jianping Xie at the NUS. His current research interests are centered on the structure prediction of metal nanoclusters with the assistance of machine learning algorithms.

Yitao Cao

Dr Yitao Cao received his BS degree (2012) from Nanjing University. He obtained his PhD degree (2017) from the University of Chinese Academy of Sciences under the supervision of Prof. Tierui Zhang. He then joined Prof. Jianping Xie's group at the National University of Singapore as a Postdoctoral Research Fellow from 2018 to 2023. In 2023, he joined Prof. Ya-Qian Lan's group at the School of Chemistry, South China Normal University. He is now interested in the stoichiometric surface chemistry of inorganic nanoclusters including POMs and metal nanoclusters.

Tiankai Chen

Dr Tiankai Chen is currently an assistant professor at the School of Science and Engineering at the Chinese University of Hong Kong, Shenzhen. He obtained his BS degree from Peking University in 2014 and PhD degree from the National University of Singapore in 2018. He has developed a variety of methods for the synthesis of metal nanoclusters and gained mechanistic insights into their growth processes. His current research interests involve the atomic-precise synthetic chemistry of nanomaterials and the application of mass spectrometry techniques.

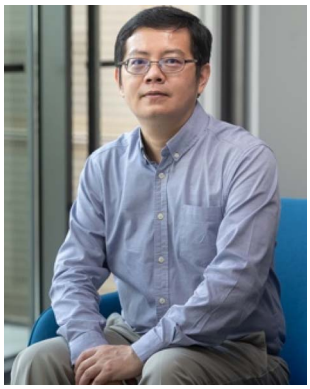

Jianping Xie

Dr Jianping Xie is a professor at the Department of Chemical & Biomolecular Engineering, National University of Singapore. He received his BS and MS from Tsinghua University and his PhD from the Singapore-MIT Alliance. Since joining the NUS in 2010, he has led research on water-soluble noble metal nanoclusters for biomedical and catalytic applications. With 280+ publications, 35 000+ citations, and an H-index of 102, he has been recognized as a Highly Cited Researcher (2018–2024, Clarivate). His interests include luminescent metal nanoclusters, nanomedicine, and nanocatalysis. He is an Associate Editor of Aggregate (Wiley).

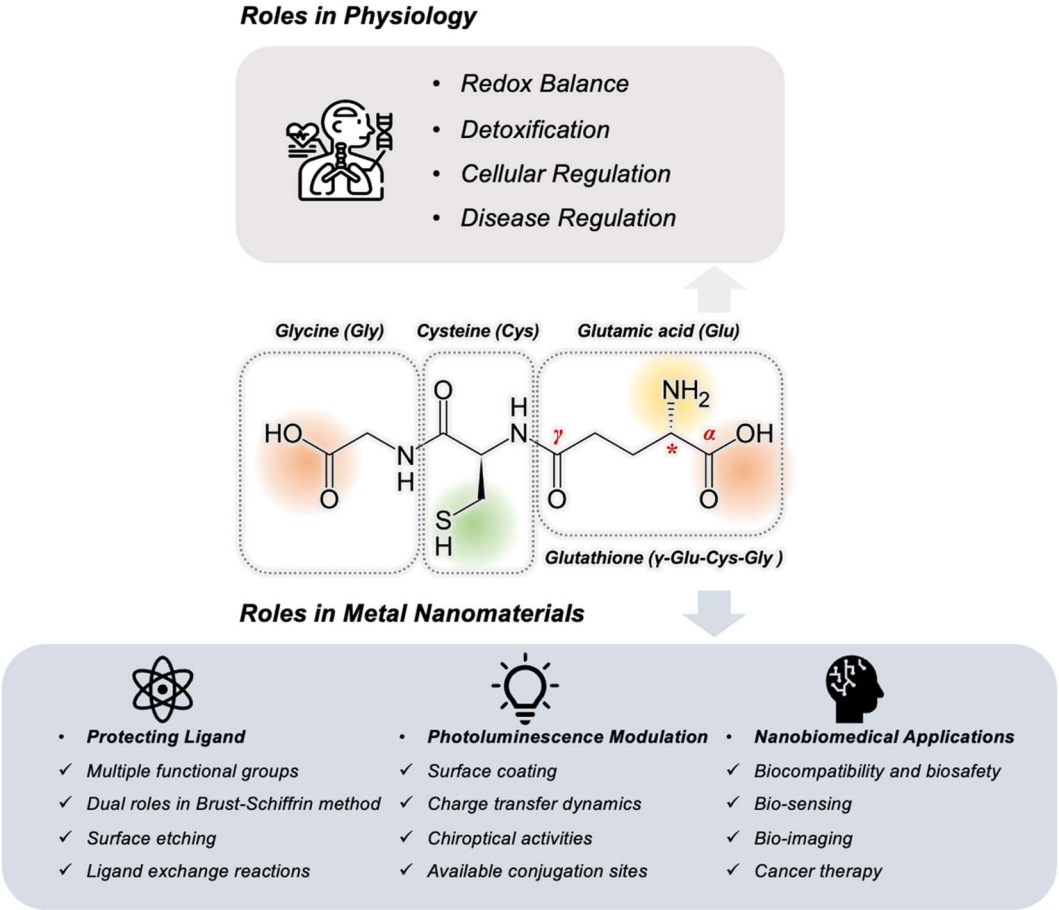

Fig. 1 Schematic illustration of the chemical structure of GSH (top panel), where multiple functional groups have been highlighted in color. And a summary of the diverse roles of GSH in physiology (middle panel) and the extension to functional metal nanomaterials (bottom panel).

antioxidant capabilities, GSH is indispensable in the detoxification process.[13,14] It conjugates with various xenobiotics, rendering them more water-soluble and facilitating their excretion from the body. This detoxification function is particularly crucial in the liver, where GSH conjugates with toxins *via* the catalytic activity of glutathione *S*-transferases (GST), thereby safeguarding cells from potentially harmful substances.[15] The significance of GSH also extends to cellular regulation, where it modulates numerous signaling pathways.[16,17] A prominent example is its role in the regulation of apoptosis, as reduced intracellular GSH levels can serve as a determining factor in initiating programmed cell death. This regulatory role is essential for normal cellular turnover and for the prevention of diseases such as cancer, where impaired apoptosis can result in unchecked cellular proliferation. The role of GSH in disease regulation has been a significant area of research.[18,19] It is well-established that dysregulated GSH levels are implicated in numerous pathologies, including neurodegenerative disorders such as Parkinson's[20,21] and Alzheimer's,[22,23] cardiovascular diseases, and certain cancers. Under these conditions, both GSH deficiency and imbalances in the GSH/GSSG ratio are critical factors contributing to disease progression. Consequently, GSH serves not only as a biomarker for oxidative stress and cellular health but also as a potential therapeutic target for various diseases.[24]

Beyond its dynamic physiological functions, GSH has promising applications in the synthesis and functionalization of various nanomaterials. This transition from physiology to materials science highlights an exciting frontier in nanotechnology, where GSH acts as a versatile protecting ligand and plays a crucial role at the bio–nano interfaces. GSH has garnered significant attention in nanomaterial synthesis due to its capacity to form stable covalent bonds with metals *via* its multiple coordination groups (–SH and –COOH).[25,26] This characteristic renders GSH an ideal candidate for stabilizing a range of nanomaterials, including quantum dots (QDs),[13,27] lanthanide nanoparticles (LNPs),[28,29] and noble metal nanoparticles (MNPs).[30,31] Remarkably, the exceptional protective properties of GSH enable the synthesis of ultra-small atomically precise metal nanoclusters (MNCs),[32–34] typically less than 3 nm in size, which demand robust stabilization due to their high surface energy. Moreover, photoluminescence (PL) is one of the most fascinating properties of these metal nanomaterials, which is a prerequisite for diverse downstream applications. Though these emissions follow excitation-decay behaviors of carriers and are fundamentally decided by the metallic parts, GSH as ligands can greatly influence the PL of these metal nanomaterials. For example, its superior coordination ability and bulky molecular structure result in enhanced passivation of

QD surfaces, reducing defects and improving quantum yields (QYs) in the emission model of QDs.[35] Furthermore, the electron-rich functional groups of GSH allow it to act as a strong electron donor, promoting charge transfer processes in metal nanomaterials compared to other ordinary ligands.[36]

The concept of an "Inseparable Duo" aptly describes GSH-protected metal nanomaterials, where the ligand GSH and the metal core synergistically target specific applications, particularly in nanobiomedicine. One of the primary advantages of the GSH ligand is its superior biosafety and biocompatibility compared to other hydrophilic modifications like polyethylene glycol (PEG) or cyclodextrins. Although PEGylation is frequently employed to improve the solubility and circulation duration of NPs within the bloodstream, it faces challenges such as the "PEG dilemma", where the immune system gradually identifies and eliminates PEGylated NPs.[37] Conversely, as a naturally occurring tripeptide, GSH is less prone to eliciting an immune response, thereby extending circulation times and minimizing nonspecific accumulation within the body. Moreover, the functional groups in GSH not only stabilize metal surfaces but also serve as responsive sites for bio-imaging[9,38,39] and bio-sensing.[15,40,41] This feature enables the "recognition" of targeting ligands, therapeutic agents, or other functional molecules, facilitating the development of multifunctional nanomaterials in precise medicine. For example, GSH-protected MNPs can be designed to selectively target specific cells or tissues, deliver therapeutic agents, and simultaneously monitor the therapeutic process *via* imaging, all integrated within a single platform.[42] Significantly, the incorporation of GSH on the surface of NPs can promote cellular uptake and improve stability within biological environments. As a result, GSH-protected metal nanomaterials are highly advantageous for anti-cancer strategies such as photothermal therapy (PTT),[43–45] photodynamic therapy (PDT),[46,47] and radiotherapy (RT).[48–50] Though the fundamental mechanisms are intrinsically decided by the features of the metallic part, GSH is preferred as the ligand for improved performance.

In this *perspective*, we aim to provide a comprehensive overview of utilizing GSH as a ligand for the development of functional metal nanomaterials. First, we delve into the synthetic fundamentals of GSH-protected metal nanomaterials, with particular emphasis on the synthesis and functionalization of QDs, MNCs, MNPs, and LNPs. Second, we highlight the modulation of PL properties in GSH-protected nanomaterials, where molecular level insights into the roles of GSH could be conducive to future designs. Third, we summarize the nano-biomedical applications of GSH-protected nanomaterials as theranostic tools, including bio-imaging, bio-sensing, and anti-cancer bio-therapies. By emphasizing this "Inseparable Duo", we aim to promote the significance of GSH in bio–nano interactions. Additionally, we propose several avenues for the future development of GSH-protected nanomaterials, ranging from the integration of smart synthesis to *in vivo* synthesis within biological systems. As research in this field advances, we foresee that the synergy between GSH and metal nanomaterials will assume an increasingly pivotal role in cutting-edge nano-biomedical applications and beyond.

2. Roles of GSH in the synthesis of metal nanomaterials

Although the targeted products may vary significantly, it is possible to summarize some general principles regarding the roles of GSH in the synthesis of these metal nanomaterials. This can be approached from the molecular perspective of the functional groups involved. The utilization of GSH primarily focuses on its thiol group, leveraging the strong metal–sulfur bonds.[51] According to classical theory on the nucleation and growth of inorganic NPs, monomers are released from metal–ligand precursors, leading to oversaturation, which subsequently results in the formation of nucleation seeds.[52] The primary role of thiols is to serve as a protective or passivating agent for the metal cores throughout the synthesis process.[53] Another notable function of thiol is serving as a sulfur donor for metal sulfide crystals, which highlights the discrepancy between "crystal-bound" and "surface-bound".[54] The thiol group also demonstrates its reducing capability in nanoscale synthesis. Notably, the Brust–Schiffrin method can be effectively divided into two stages, distinctly showcasing both the reducing capability of the thiol (*e.g.*, the reduction of Au^{3+} to Au^{+} in the first stage) and its protective role throughout the entire process.[55] More interestingly, this method was later well transformed to synthesize ultra-small MNCs.[56] Besides, the strong coordination with the metal of GSH is also used to design novel synthesis strategies, such as surface ligand etching and ligand exchange reactions.[41,57–59] These strategies are often utilized to expand both the synthesis boundaries and the diverse functionalities of nanomaterials. On top of thiol groups, it should not be neglected that other functional groups can offer "weak" interactions that contribute to delicate surface control and interparticle crosslinking, as demonstrated in some cases of some Au NPs and LNPs.[28,60]

This section aims to summarize the fundamentals of the ligand in the synthesis of GSH-protected metal nanomaterials from a molecular perspective, namely the protecting ligand with multiple functional groups, dual roles in the Brust–Schiffrin method, surface etching, and ligand exchange reactions mediated by GSH. Table 1 provides a summary, categorizing representative GSH-protected metal nanomaterials based on the specific roles GSH plays during their synthesis.

2.1 Ligands with multiple functional groups

Among the various synthesis methods for QDs of different sizes, the thermal decomposition method is the decomposition of organometallic compounds containing chalcogenides and metals that are employed as precursors in high-boiling organic solvents at relatively high temperatures (~300 °C). To achieve this, a crucial aspect is the rapid nucleation step at the initial stage of the reaction, followed by controlled nucleus growth while suppressing any further nucleation.[74] However, using water-soluble thiol ligands like GSH offers two significant advantages compared to the organometallic technique: a stronger binding affinity between the thiol ligand and the NP surface compared to trioctylphosphine oxide, and the ability to

Table 1 Summary of the roles of GSH in synthesis of metal nanomaterials

Roles	Functional groups	Examples
Multiple functional groups	–SH only	CdSe QDs,[61] ZnS QDs,[62] $Au_{22}(SG)_{18}$,[26] and Au NPs[22]
	–COOH only	LNPs[28]
	–COOH and $–NH_2$ are involved	AIS QDs (for surface coverage),[63] ZnSe/ZnS QDs (*in situ* growth core–shell structure),[64] and Au NPs (for surface coverage)[60]
Dual roles in the Brust–Schiffrin method	Protecting and reducing through –SH	$Au_{25}(SG)_{18}$,[65] $Au_{10-12}(SG)_{10-12}$, $Au_{15}(SG)_{13}$ and $Au_{18}(SG)_{14}$,[25] Au NPs,[66] and Au/Ag bimetallic NPs[67,68]
Surface etching	–SH	Intercluster transformation between $Au_{10-12}(SG)_{10-12}$, $Au_{22}(SG)_{18}$, $Au_{15}(SG)_{13}$, and $Au_{18}(SG)_{14}$,[57] Ag QDs etching to Ag NPs,[69] $Ag_{16}(SG)_9$, and $Ag_9(SG)_6$ (ref. 70)
GSH-mediated ligand exchange reactions	–SH	PbS QDs[71,72] and CIS_2 QDs[73]
		Intercluster transformation between $Ag_{35}(SG)_{18}$, $Ag_{37}(SG)_{21}$ and Ag_{44}(4-fluorothiophenol)$_{30}$ (ref. 59)
		$Au_{15}(SG)_{13}$, and $Au_{15}(SG)_{12}Ao$[41]

induce immediate nucleation at low temperatures, followed by steady crystal growth as the temperature increases.[75] In addition to these advantages, several other notable features, such as accessibility, biocompatibility, versatility, and low-temperature activity, further enhance the superiority of this process compared to the methods mentioned earlier.

With these advantages, GSH plays an important role in synthesizing QDs with high QYs. For instance, GSH-protected CdSe QDs were synthesized with a high QY of 16% and a small full width at half-maximum, offering improved performance compared to previous aqueous QDs.[27] Although direct use of GSH was extended to synthesizing ZnS[62] and CdS[76] QDs, these products performed less satisfactorily with respect to their QYs, which might be ascribed to the absence of other chalcogens besides S, such as Se or Te, as the optical properties of QDs are highly composition dependent. Later, Ren *et al.* applied this method to CdTe synthesis with modifications, achieving a maximum QY of 62% at 525 nm.[77] The presence of GSH was found to significantly influence the Ostwald ripening mechanism, with lower pH levels slowing particle growth. Optimal QY was obtained at a pH of 8 and a reaction time of 30 minutes. In another study, CdTe QDs were synthesized with tunable emissions by adjusting their heating timespan.[9] The same group developed ZnCdSe alloyed QDs capped with GSH and achieved a maximum QY of 50%, which surpasses that of the previously reported CdSe QDs.[78] Moreover, leveraging GSH's ability to form polymerized crosslinks, or phytochelatin, Ying *et al.* synthesized intramolecular crosslinked GSH-protected CdTe QDs. The surface passivation by interlinked GSH enhanced the stability of the product and facilitated its functionalization with bioprobes.[79]

We would like to emphasize that thiols occupy a unique category of ligands, as they can concomitantly act as the sulfur source in the synthesis of metal sulfide nanocrystals (while this could induce chalcogenide contamination if not targeting metal sulfides). At high temperatures, thiols decompose at the metal center, producing metal sulfide and an alkene.[80] This highlights the intriguing diversity of bonding types present on the surface of nanocrystals. When thiols only serve as ligands, they are bound to metal cations at low coordination number surface sites, which we describe as "surface-bound". The protecting thiols that result from reactions where they are also the sulfur source become the terminal layer of sulfurs of the crystal. These thiols are exceptionally strongly bound because they sit in high coordination number sites; they are the so-called "crystal-bound" thiols.[54]

While the surfaces of QDs are passivated by thiol groups, other functional groups in GSH could also be active, particularly in subsequent growth stages toward the formation of more complex structures. In a representative case, the soft acid Ag^+ will interact with the thiol group of GSH to form a coordination complex chain (–SG–Ag–SG–). Following the hot injection of Na_2S, the intermediate Ag_2S is formed, which subsequently undergoes cation exchange with In^{3+}, to yield AgInS (AIS) QDs through the reaction ($2Ag_2S + In^{3+} \rightarrow AgInS_2 + 3Ag^+$) as shown in Fig. 2a.[81] GSH serves both as a protective agent and as an anchoring site for the growth of the ZnS shell (*via* –COO–Zn interactions) on the surface of the core AIS QDs. Although Na_2S is added as a sulfur source, the Zn precursor solution contains additional GSH surface ligands to ensure full coverage and colloidal stability of the core–shell QDs. Thus, the primary role of GSH is as a protective ligand facilitating surface passivation. Additionally, GSH functions as a bridging agent for subsequent *in situ* growth, as demonstrated in core–shell ZnSe/ZnS QDs and ZnAgInS (ZAIS) QDs encapsulated within metal–organic frameworks (MOFs).[82] On top of the involvement in structure configuration modulation, the weak anchoring sites of $–NH_2$ and –COOH groups also participate in delicate surface coordination. For instance, GSH-protected Au NPs provide valuable chemical insights into the intricate design of multiple anchoring points, though being trivial in contrast to Au–S ($\approx$40 kcal mol^{-1}), and the weak interactions of Au–N ($\approx$8 kcal mol^{-1}) and Au–O ($\approx$2 kcal mol^{-1}).[83,84] This presents an intriguing scenario where the relatively limited presence of GSH as

a protecting ligand can "activate" these weaker interactions, resulting in significantly different emission properties, even among Au NPs of similar diameters (Fig. 2b).[60] Another notable class of GSH-protected metal nanomaterials that may not rely on metal–sulfur bonds is LNPs, where –COOH groups are more favorable for interaction with lanthanide cations. In this context, GSH, an endogenous tripeptide with two –COOH groups, coordinates with lanthanide cations, while the thiol group can be oxidized by ROS to form disulfide bonds (–S–S–). As a result, ROS-responsive cross-linking between GSH-protected nanomaterials can be specifically triggered in inflamed areas as shown in Fig. 2c.[28]

2.2 Dual roles in the Brust–Schiffrin method

The diverse roles of GSH in the synthesis of metal nanomaterials are never demonstrated better in any synthetic method than the Brust–Schiffrin method. Specifically, GSH's

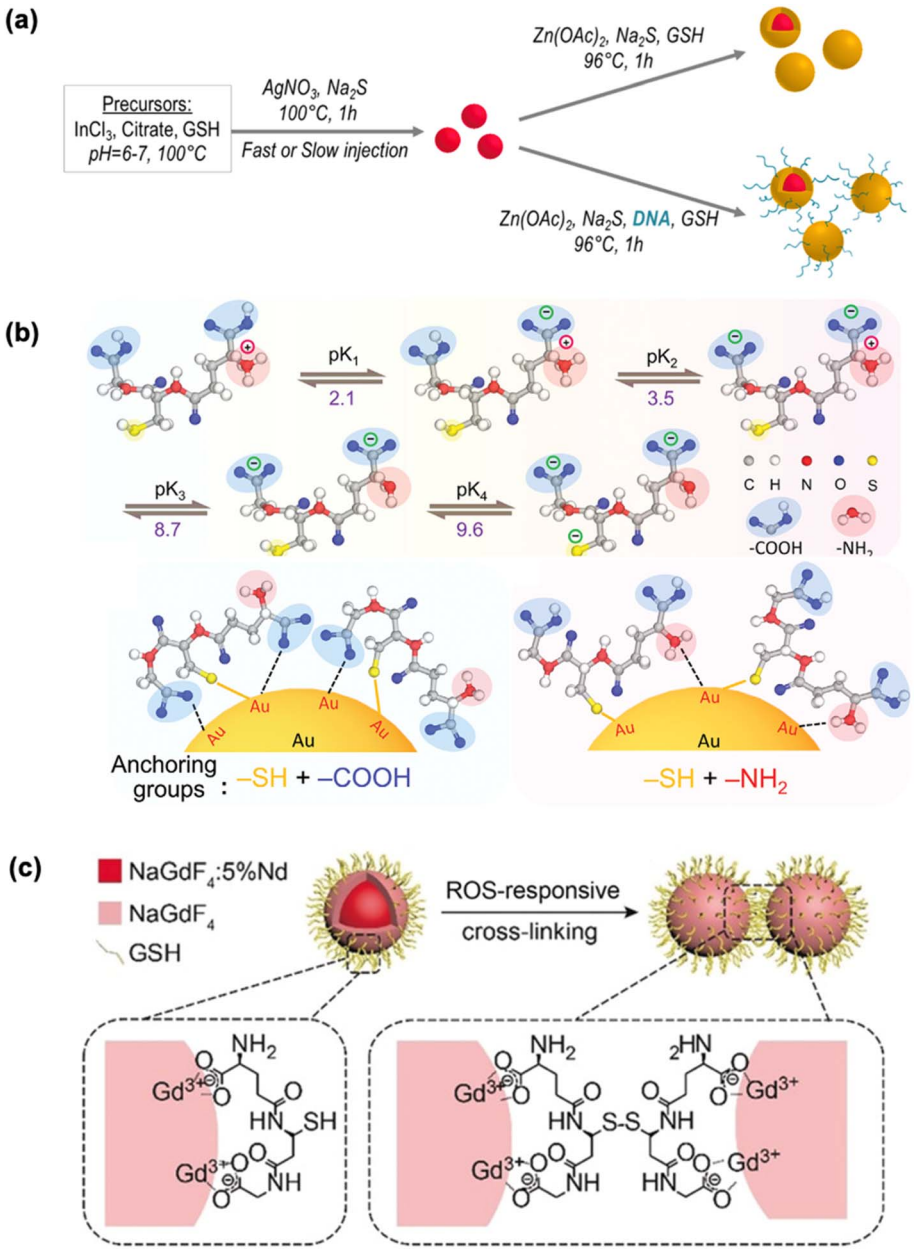

Fig. 2 Synthesis or functionalization of GSH-protected metal nanomaterials enabled by multiple functional groups. (a) Schematic representation of the aqueous synthesis strategy for AIS_2/ZnS core/shell QDs functionalized with DNA, where GSH is used as a linker for shell growth. Reprinted with permission from ref. 81. Copyright 2020 American Chemical Society. (b) Schematic illustration of step-wise ionization and activation of functional groups of GSH, and the GSH-protected Au NPs synthesized at pH 10.0 (left panel) and pH 2.0 (right panel). Reprinted with permission from ref. 60. Copyright 2021 Wiley. (c) Schematic illustration of bioimaging for acute local epidermal inflammation using the reductive –SH in GSH–protected LNP nanoprobes. The nanoprobes cross-link at the inflamed site in response to ROS and are rapidly excreted from the body. Reprinted with permission from ref. 28. Copyright 2019 Wiley.

dual function as both a reducing and protecting agent highlights its versatility, making it one of the most valuable ligands in nanomaterial synthesis. In a typical "two steps in one pot" synthesis, when $HAuCl_4$ is mixed with GSH, the thiol group of GSH reduces Au^{3+} to Au^{+} in the first step. This reaction results in the formation of Au–SG complexes and oxidized GSSG.[55] This reaction is typically represented by using the following equation:

$$Au^{3+} + 3GSH \rightarrow Au\text{–}SG + GSSG.$$

The thiol group of GSH donates two electrons to the gold center, reducing Au^{3+} to Au^{+} while simultaneously forming a disulfide bond between two GSH molecules, yielding GSSG. The resulting Au–SG complexes exhibit considerable stability due to the strong gold–sulfur interaction, which is less susceptible to oxidation compared to Au^{3+}. Thus, the Au–SG complex remains relatively stable in comparison to its Au^{3+} precursor.[85] The robust gold–sulfur bond, combined with the bulky size of GSH and its ability to form intermolecular hydrogen bonds (between H-donors such as –OH and $–NH_2$, and H-acceptors such as C=O), allows GSH to protect gold precursors more effectively than other water-soluble ligands. The strong Au–S bond between the gold atom and the thiolate group of GSH plays a critical role in stabilizing the gold precursor. The sulfur atom in GSH donates electron density, thereby stabilizing the Au^{+} center and preventing further oxidation. This steric protection serves to shield the gold core from external oxidants, contributing to the stability of the Au–SG complex. This protection continues until the addition of a reducing agent (*e.g.*, $NaBH_4$). The described method highlights the significant progress in nanoscience, transitioning from the synthesis of Au NPs to atomically precise MNCs. This advancement in synthetic techniques represents a key development, pushing the frontier of nanoscience by enabling more controlled and precise nanomaterial structures. Whetten *et al.* first reported atomically precise Au NCs formulated as $Au_{28}(SG)_{16}$, which was later corrected as $Au_{25}(SG)_{18}$.[65,86] Remarkably, Tsukuda *et al.* obtained a series of GSH-protected Au NCs *via* polyacrylamide gel electrophoresis separation and further determined the formulae by mass spectrometry.[87] Among this series, $Au_{25}(SG)_{18}$ was found to have a particularly high stability against etching. Bigioni *et al.* extended the synthesis to a series of GSH-protected Ag NCs, and many of them have been structurally confirmed in later studies.[88] This method emphasizes the adaptability of the Brust–Schiffrin method over recent decades, showcasing advancements such as the switch from two-phase to water-phase synthesis, modifications in reducing capabilities (involving reducing agents, pH, and temperature), and optimization of precursor configurations like the thiol-to-metal ratio.

First, due to the presence of –COOH and $–NH_2$ groups, metal(I)–SG complexes can exhibit different conformational states at different pH values that can decide the products.[66] In a modified Brust–Schiffrin method, size-controllable synthesis of Au NPs 6 to 2 nm in diameter by adjusting pH from 5.3 to 8 was reported, following the mechanism proposed as shown in Fig. 3a. Besides, the reducing power of the reducing agents is closely influenced by the pH. By merely adjusting the reaction pH to 2 or 2.7, Xie *et al.* managed to synthesize $Au_{15}(SG)_{13}$ or $Au_{18}(SG)_{14}$ of high purity, respectively.[92] Notably, the amount of $NaBH_4$ to selectively synthesize $Au_{25}(SG)_{18}$ was stoichiometrically determined to be Au-to-e^- = 32 : 8 by the same group, which significantly improved the precision in the Brust–Schiffrin method (Fig. 3d).[90] A milder reducing agent, carbon monoxide, was developed for the one-pot production of different-sized Au NCs of high purity by pH adjustment, as depicted in Fig. 3b.[25] Adjusting the pH to 7, 9, 10, and 11 results in the formation of $Au_{10–12}(SG)_{10–12}$, $Au_{15}(SG)_{13}$, $Au_{18}(SG)_{14}$, and $Au_{25}(SG)_{18}$, respectively. This trend in size is interestingly opposite to that observed with $NaBH_4$, indicating distinct chemical equilibriums that are heavily dependent on the concentration of OH^-. Upon adjusting this protocol, $Au_{22}(SG)_{18}$, a highly luminescent star molecule was produced, which emits at 665 nm with a QY of 8%.[26]

Second, when the thiol-to-gold ratio is excessively high, only short Au(I)–SG complexes with low curvature are formed, typically resulting in larger Au NPs. Therefore, only an optimal thiol-to-gold ratio is necessary to achieve the formation of smaller NPs (Fig. 3c).[89] For example, orange and yellow emitting NPs were obtained using a GSH-to-Au ratio of 1 : 1 and 2 : 1, respectively.[93] Although the orange-emitting NPs, with a size of approximately 1.7 nm, are smaller than the yellow-emitting NPs, which have a size of 2.1 nm, their QY remains comparable, with both around 4%. A later study then varied the GSH-to-Au ratio from 0.8 to 1.6 and synthesized NPs of the same size ~2.5 nm exhibiting different emission behaviors.[84] The emission wavelength varied from 810 nm at a GSH-to-Au ratio of 0.8 to 600 nm at a ratio of 1.6. While this study highlighted the importance of the GSH-to-Au ratio in determining product size, readers may observe the inconsistent use of ratios, even in the synthesis of the same product. Admittedly, the relationship between the stoichiometry of GSH-to-Au and the final products remains unclear and requires further investigation for comprehensive understanding.

Third, while the conventional Brust–Schiffrin method utilizes a strong reducing agent, $NaBH_4$, GSH can fulfill this role as a milder reducing agent under heating. Notably, this heating approach often leads to a mixture of highly luminescent species, though at the expense of prolonged reaction times, likely due to the increased motif length of the resulting nanomaterials.[94] In the case of the aforementioned emissive Au NPs, synthesis was achieved by heating at 95 °C. This mild reduction method was later extended by the same group to the synthesis of bi-ligand Au NPs, Ag NPs, and Au/Ag bimetallic NPs.[67,68] Similarly, GSH was used to produce highly luminescent Au NCs. Facilitated by heating and a low GSH-to-Au ratio of 1.5, Xie's method produced cluster species with a QY of 15%.[95] As shown in Fig. 3e, a recent advancement in data-driven synthesis of highly emissive GSH-protected Au NCs also utilizes this heating strategy without the addition of other reducing agents, revealing the complex correlations between QYs and multi-dimensional synthesis parameters like temperature, ratio, and time.[91]

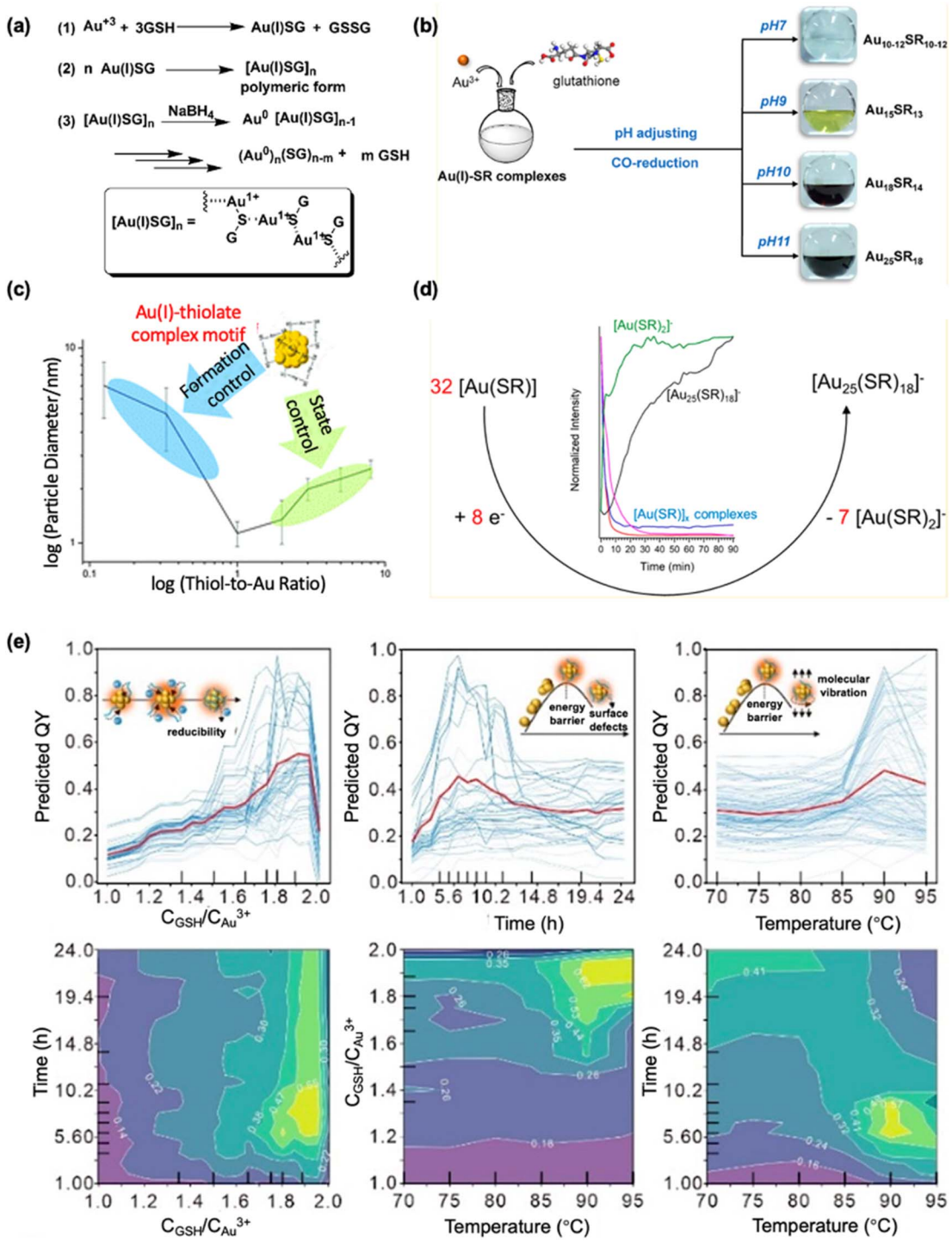

Fig. 3 Dual roles of GSH and parameter space in the Brust–Schiffrin method. (a) Proposed mechanism for the formation of Au NPs from Au^{3+} and GSH. Reprinted with permission from ref. 66. Copyright 2008 American Chemical Society. (b) Schematic illustration depicting the production of Au_{10-12}, Au_{15}, Au_{18}, and Au_{25} NCs by adjusting the pH of the reaction solution in the CO-reduction method. Reprinted with permission from ref. 25. Copyright 2013 American Chemical Society. (c) A U-shape trend is identified between the size of Au NPs and the thiol-to-Au ratio. Reprinted with permission from ref. 89. Copyright 2016 Royal Society of Chemistry. (d) Synthesis of water-soluble $Au_{25}(SR)_{18}$ using a stoichiometric amount of $NaBH_4$. Reprinted with permission from ref. 90. Copyright 2018 American Chemical Society. (e) Explainability of machine learning studies of complex correlations among synthetic parameters for GSH-protected Au NCs. Reprinted with permission from ref. 91. Copyright 2023 Royal Society of Chemistry.

2.3 Surface etching by GSH

Etching adopts a "top-down" approach to generate smaller metal nanomaterials by removing metal atoms from the larger counterparts,[96–98] upon forming thiolate radicals in the presence of oxygen.[99] GSH has been used to produce smaller nanomaterials from larger ones following this top-down synthetic process toward thermodynamically preferred species.

Pradeep *et al.* implemented an additional ligand etching step following the synthesis of $Au_{25}(SG)_{18}$ using a modified Brust–Schiffrin method where precursors and the reaction mixture were cooled to 0 °C for better purity.[100] The same group also succeeded in synthesizing $Au_{25}(SG)_{18}$ from mercaptosuccinic acid-protected large Au NPs upon etching with excess GSH.[101] Moreover, Yang *et al.* successfully synthesized a series of GSH-protected Au NCs by the etching method. The sensitivity of the cluster transformation to surface modifications demonstrated in this study provides valuable insights into predicting the behavior and fate of MNCs in various fields.[57] The idea was further extended to other noble metals by Schneider *et al.* who successfully synthesized GSH-protected Pt NCs with yellow emission[102] and highly luminescent Ag NCs exhibiting a QY exceeding 60%.[103] Besides, highly luminescent Ag NCs can be synthesized *via* a cyclic reduction-decomposition method as shown in Fig. 4c.[70] Upon the initial addition of NaOH-mediated $NaBH_4$, the mixture was incubated at room temperature for 3 hours, allowing GSH to etch the unstable Ag NC intermediates. The same reducing agent was added again, followed by another incubation period. Depending on the amount of $NaBH_4$ and the duration of incubation, two luminescent species, $Ag_{16}(SG)_9$ and $Ag_9(SG)_6$, were produced, with emission peaks at 647 nm and 495 nm, respectively.

Additionally, it is important to note that the etching mechanism is nearly ubiquitous in nanoscale synthesis. For instance, thiol etching can act as a shuttle between different NPs, facilitating composition exchange. A critical limitation in the assembly of Ag NPs and QDs was revealed: the equilibrium desorption of thiol ligands from QDs leads to the etching of Ag NPs, the formation of silver–thiol ligand complexes, and the quenching of QD emission through trap-inducing cation exchange reactions (Fig. 4a).[69] Moreover, novel MNCs and intercluster transformation could be achieved by etching reactions, where some kinetically favored species diminish for high purity of desired products. As early as 2007, Tsukuda *et al.* revealed the concept of "natural selection" based on stability against etching, which has further guided the development of one-pot synthesis methods aimed at producing high-quality products (Fig. 4b).[58] Thus, adjustments of parameters such as pH and temperature can facilitate the etching process, as demonstrated in the following cases.[104] NaOH was introduced to accelerate the etching reaction by GSH, promoting the formation of the thermodynamically favorable Au_{25} species with high purity.[85] In the absence of NaOH, the reaction can also be

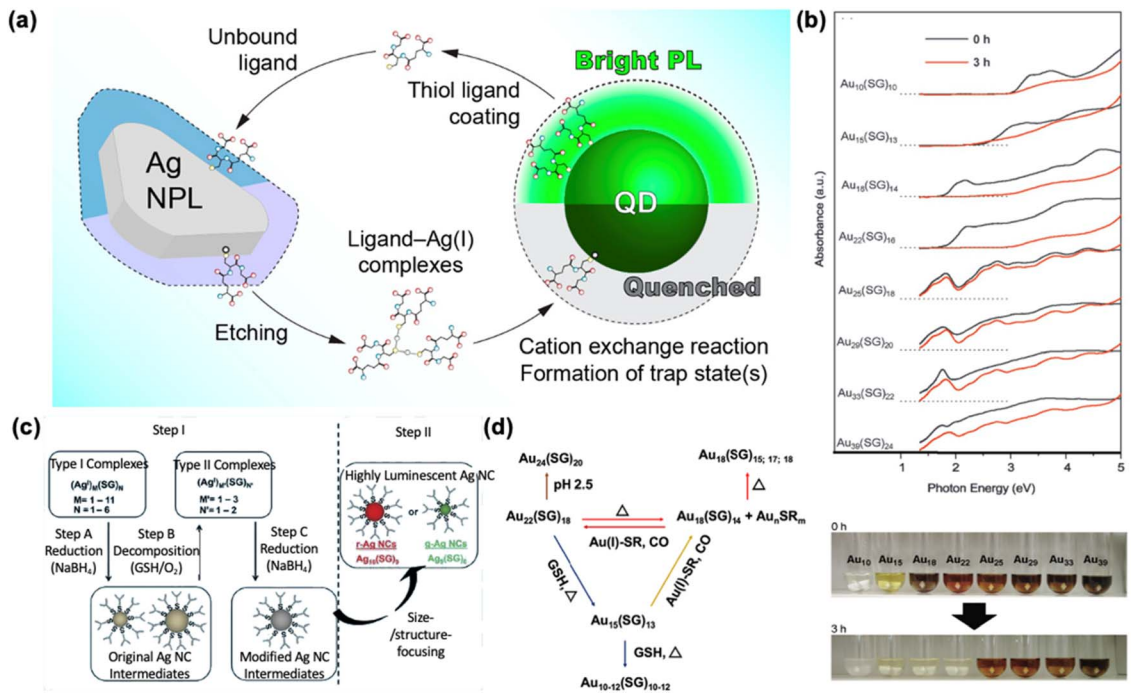

Fig. 4 Roles of GSH in surface etching of metal nanomaterials. (a) Proposed mechanism for gradual quenching of QD PL and etching of Ag NPs upon mixing. Reprinted with permission from ref. 69. Copyright 2017 American Chemical Society. (b) Etching of different sized Au NCs by GSH toward species with higher stability and the color changes of aqueous solution Au NCs, respectively. Reprinted with permission from ref. 58. Copyright 2007 Wiley. (c) Schematic illustration of the process for generating highly luminescent GSH-protected Ag NCs in the aqueous phase. Reprinted with permission under a Creative Commons CC-BY-NC-ND License from ref. 70. Copyright 2013 The Authors. (d) Schematic illustration of the interconversion process among GSH-protected Au NCs. Reprinted with permission from ref. 57. Copyright 2020 American Chemical Society.

accelerated by heating.[105,106] For instance, heating at 60 °C leads to the formation of $Au_{25}(SG)_{18}$ within 2 hours. Notably, a recent study highlighted the significance of surface sensitivity of GSH-protected Au NCs in intercluster transformation (Fig. 4d), where etching is a major avenue to selected products.[57]

2.4 Ligand exchange reactions mediated by GSH

Ligand exchange reactions have been extensively utilized as a post-modification strategy to introduce new ligands and improve the surface properties of parent NCs without altering the metal core. GSH facilitates ligand exchange reactions, either as an attacking free ligand or more commonly as the existing ligand, particularly in cases where direct synthesis of the desired nanomaterials is challenging.

The involvement of GSH in ligand exchange reactions not only imparts superior biocompatibility to the product but also enhances the phase transfer and stability of QDs. For instance, the ligand exchange of PbS QDs with the multi-chelating L-GSH retained approximately 70% of the emission intensity of oleate-protected QDs and exhibited excellent stability, maintaining its properties for over 20 days under ambient conditions (Fig. 5a).[71] The multiple chelating sites of GSH, combined with potential surface passivation through secondary coordination to Pb surface sites, contribute to the efficient ligand exchange and long-term stability of PbS QDs.

For atomically precise MNCs, GSH-mediated ligand exchange reactions significantly broaden the cluster library. Variations in the protective capability of different ligands over the metal core result in the formation of nanomaterials with distinct stable sizes.[85] Consequently, GSH-involved ligand exchange reactions were conducted to induce variations in core size. The first report of ligand exchange between hydrophobic ligand-protected Au NCs and GSH was presented by Tsukuda *et al.*, who reacted phosphine-stabilized Au_{11} clusters in chloroform with an aqueous GSH solution under aerobic conditions (Fig. 5b).[107] The reaction selectively produces $Au_{25}(SG)_{18}$ with high purity, attributed to GSH's capacity to induce the aggregation of phosphine-protected Au NCs. This explanation was subsequently refined by Hutchison *et al.*, who highlighted the low stability of phosphine-protected precursors.[108] Importantly, GSH-protected MNCs serve as the parent material for further diversification. A straightforward method for synthesizing Au_{38}(1-dodecanethiol)$_{24}$ with high purity and yield was developed by introducing 1-dodecanethiol to the GSH-protected Au NC precursor in a two-phase reaction system.[109] In another study, Zhu *et al.* exchanged the flexible GSH ligands of $Au_{18}(SG)_{14}$ with rigid cyclohexanethiolate.[110] The new thiolate-protected Au_{18} cluster facilitated the investigation into its growth mechanism and crystal structure identification. $Au_{15}(SG)_{13}$ was also used as a precursor in the synthesis of Au_{16}(1-adamantanethiolate)$_{12}$ (ref. 111) and Au_{16}(2-phenylethanethiol)$_{14}$.[112] This was also applied in Ag NCs where $Ag_{35}(SG)_{18}$ can produce clusters of different core sizes with different ligands.[59] Notably, the reversible transformation between $Ag_{35}(SG)_{18}$ and Ag_{44}(4-fluorothiophenol)$_{30}$ NCs has been observed. The authors employed a recently developed theory of reverse Ostwald ripening to model this interconversion, emphasizing the critical role of subtle changes in ligand–metal binding energy. These findings illustrate how GSH, serving as a protective ligand, can significantly influence the equilibrium size of the resulting NCs (Fig. 5c).

Notably, researchers have been investigating the detailed mechanisms of ligand exchange reactions, both experimentally and theoretically, facilitated by the atomic precision of MNCs.[41,85,107,108,113] For instance, recent studies have shown that ligand exchange is site-specifically enabled by the flexible gold–sulfur interface on the surface motif of MNCs, normally following a S_N2-like mechanism.[114] We envision that more atomic-level insights could be implemented to enable diverse functionalization and modification of metal nanomaterials.

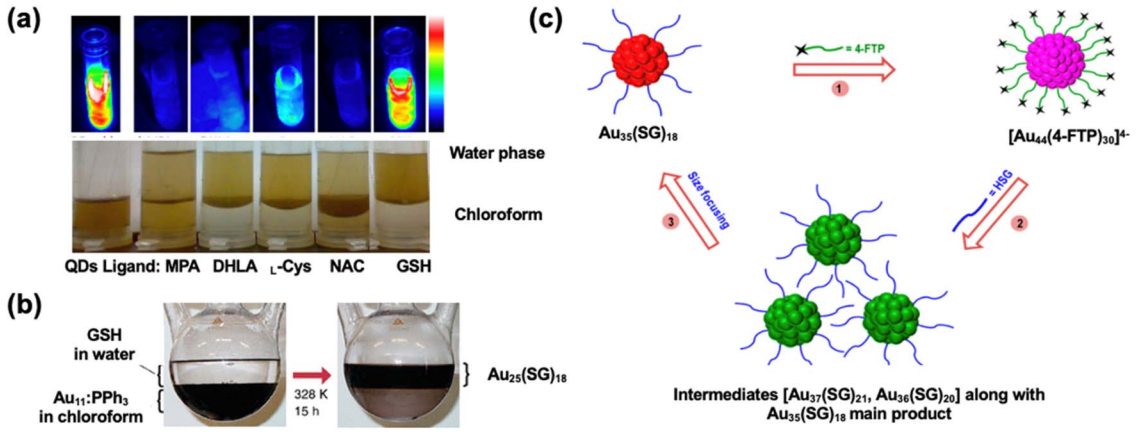

Fig. 5 Representative ligand exchange reactions facilitated by GSH. (a) Photographs of the original QD solution and the phase transfer experiments using different ligands under visible and NIR laser light. Readapted with permission from ref. 71. Copyright 2011 Elsevier Inc. (b) GSH transfer Au NCs from the organic phase to the water phase. Reprinted with permission from ref. 107. Copyright 2005 American Chemical Society. (c) Reversible transformation of $Ag_{35}(SG)_{18}$ into Ag_{44}(4-FTP)$_{30}$. Reprinted with permission from ref. 59. Copyright 2015 American Chemical Society.

3. Regulation of optical properties of GSH-protected metal nanomaterials

As highlighted in the concept of "Inseparable Duo" of GSH-protected metal nanomaterials, they could exhibit interesting optical properties owing to their metallic compositions. Though these optical properties, such as PL and circularly polarized luminescence (CPL) responses, could be largely attributed to the metallic part, no one would say that the ligand has barely any effect during the processes. The roles of GSH as the ligand could be very significant in tuning the optical properties, and we aim to discuss them at the molecular level in this section.

First, surface defects are a critically negative issue in the size-dependent emission of QDs, while the multiple coordination capability of GSH could help improve the QYs. Besides, strategies to improve QYs also rely on the "bridging" effect of GSH by coating shell QDs onto the core QDs, especially in the cases simultaneously using a thiol group for the core and –COOH group for the ZnS shell.[115] Not to mention the drastic emission variations induced by coordination in the cases of Au NPs.[84] Second, atomic-level understandings are enabled with atomically precise MNCs, where the ligand effect and charge transfer dynamics could be revealed with the help of advanced PL evaluation. GSH is designated as an electron-rich donor that is beneficial to PL enhancement of MNCs,[14] which further helps the build-up of the concept of aggregation-induced emission (AIE) in MNCs.[94] Third, GSH is a chiral molecule and could transfer the chirality from itself to the assembled GSH-protected nanomaterials to induce CPL responses.[116,117] This is not only interesting for designing the optical properties but also crucial to safe and effective bio-applications in the next step.[40,118,119] Last, though some of the functional groups are employed in stabilizing the nanomaterials, the other spare ones could be used as available conjugation sites for endogenous molecules for tunable emission.[120] This function is also of great significance, particularly in applications like bio-sensing and imaging.

Therefore, we would like to discuss the roles of GSH from the perspectives of surface coating, charge transfer dynamics, CPL responses, and conjugation sites. A summary is provided in Table 2 to categorize representative PL performances of GSH-protected metal nanomaterials, echoing the concept of an "Inseparable Duo" and highlighting the multi-faceted roles of GSH.

3.1 Surface coating

Since the initial discovery of semiconducting CdS QDs in the 1980s, the unique size-dependent emission properties of QDs have garnered significant attention.[134] Their characteristics, including narrow size distribution, high fluorescence, and excellent emission tunability, position QDs as promising candidates for commercial optoelectronic materials, chemical sensors, and bioimaging agents.[135,136] However, aqueous QDs often exhibit low QYs, surface defects, and toxicity. These issues can be partially mitigated by introducing GSH as a protecting ligand, as GSH enhances biocompatibility and provides effective surface protection.

First, one of the primary factors that reduce the QY of QDs is exposure to oxidative environments, which can be mitigated by the antioxidant properties of GSH on the surface. GSH interacts strongly with certain metal cations (*e.g.*, Zn^{2+} and Cd^{2+}), thereby enhancing the surface passivation of QDs. From a surface chemistry perspective, the unsaturated coordination of atoms on the surface of QDs leads to numerous dangling bonds. These dangling bonds necessitate essential surface coating to stabilize

Table 2 Summary of PL properties of representative GSH-protected nanomaterials

Core composition	QY(s)	Emission wavelength
CdTe[9,77]	62%	480–650 nm
ZnSe/ZnS[64]	22% (pH > 10.3)	~360 nm
CdTe/ZnS[115]	84%	569–630 nm
CdTe/CdS[121]	83%	530–588 nm
Mn-doped ZnS[122]	48%	580 nm
ZnCdSe[123]	50%	425–475 nm
Ag/Cu-doped ZnCdS[123]	31% and 21%	Full visible spectrum
CdZnTe[124]	75%	470–610 nm
PbS[71,72]	>30%	NIR-II (1000 nm)
Ag_2S[13,43]	60%	NIR-I (700–900 nm)
CIS[125]	2.8%	Tunable at 500–900 nm
CIS/ZnS[73,125]	12.3% and 34% with MPA co-protected	
AIS[126,127]	~32%	Tunable at 540–622 nm
AIS/ZnS[81,126,127]	~60%	
Au_{22} (Au NCs)[26,128]	~8%	~665 nm
TOA-rigidified Au_{22} (ref. 129)	60%	
Bis-Schiff base crosslinked Au_{22} (ref. 130)	48%	
Au_{25} (Au NCs)[87,131]	0.1%	700–800 nm and NIR-II (1100 nm)
~2.5 nm Au NPs[60,132]	<0.01%	561 nm
Ag_{16} (Ag NCs)[70,103]	4.2%	647 nm
2–3 nm Cu NPs[133]	3.08%	440 nm
Cu_{15} (Cu NCs)[38]	6%	430 nm
<2 nm Pt NCs[61]	17%	570 nm

the NPs and prevent surface defects.[137] Using CdTe as an example, the strong bonding between Cd^{2+} and GSH is believed to create a protective layer on the surface, passivating the dangling bonds from Te atoms. This improves the confinement of photogenerated charge carriers, thereby enhancing the QY of the material. With optimized pH and a higher molar ratio of Cd^{2+}-GSH/NaHTe, improved surface passivation was anticipated. A well-protected surface minimized the presence of defects, leading to a maximum QY of up to 60%.[77] A similar strategy was adopted by Ying *et al.*, who reported the successful synthesis of GSH-protected CdTe QDs with tunable emissions and high QY up to 45%, where the integration of GSH not only improves QYs but also boost cell imaging as evidenced in the con-focal fluorescence images in Fig. 6a.[9] Yu *et al.* synthesized CdSe QDs, demonstrating that compared to cysteine, the stronger binding affinity of GSH to Cd^{2+} ions significantly improved the optical properties and crystal structure of the QDs.[140]

Strategies such as employing core–shell structures or confinement can enhance the QYs of QDs. In these approaches, GSH serves not only as a surface-protecting ligand but also as an anchoring point for the *in situ* formation of outer architectures. The aqueous-phase synthesis of ZnSe QDs exhibits a pronounced pH-dependent structural evolution, underscoring the significant impact of pH on both material properties and growth mechanisms. At elevated pH levels, the deprotonation of amine groups within GSH facilitates the release of sulfur, which then contributes to the formation of ZnSe/ZnS core–shell QDs. The addition of the ZnS shell plays a vital role in enhancing the QY of the QDs, as the shell passivates surface states, reducing the density of non-radiative recombination centers. Consequently, this passivation improves both the photoluminescence efficiency and the overall optical stability of the QDs.[64] Similarly, GSH can also serve as both a protecting ligand and a sulfur source for the growth of an additional ZnS shell on the as-prepared CdTe core QDs. This was confirmed by X-ray

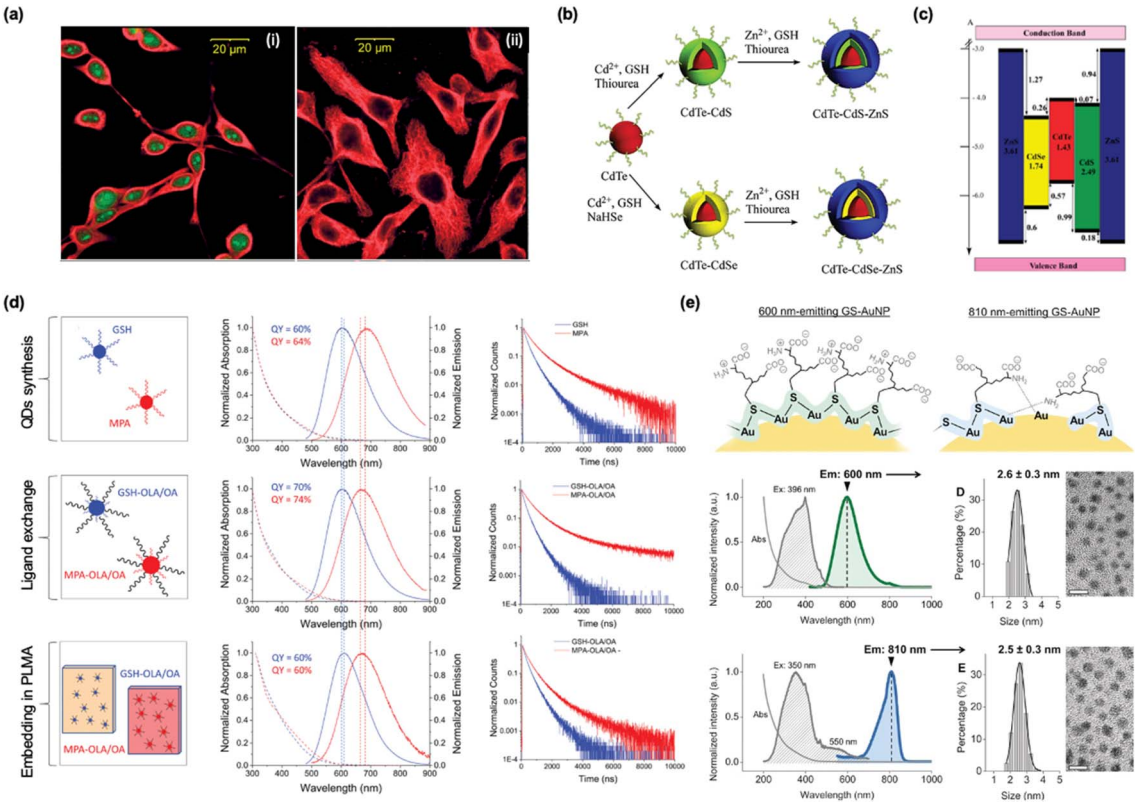

Fig. 6 Roles of surface coating in PL of GSH-protected metal nanomaterials. (a) Confocal fluorescence images of cells stained with QDs. (i) Fixed HepG2 cells with nucleoli and cytoplasm stained by GSHCdTe517 QDs (green) and GSH-CdTe618 QDs (red). (ii) Fixed NIH 3T3 cells with actin immunostained using biotin-labeled GSH-CdTe618 QDs. Reprinted with permission from ref. 9. Copyright 2007 Wiley. (b) Schematic illustration of the synthesis of CdTe/CdS/ZnS and CdTe/CdSe/ZnS core/shell/shell QDs and (c) the scheme illustrating the band offsets of CdTe, CdS, CdSe, and ZnS materials. The energy levels of the band edges are shown for bulk materials in eV. Reprinted with permission from ref. 138. Copyright 2012 American Chemical Society. (d) Schematic illustration of hydrophilic AIS/ZnS QDs capped with MPA and GSH, followed by ligand exchange to produce hydrophobic AIS/ZnS QDs capped with MPA-OLA/OA or GSH-OLA/OA, as well as hydrophobic AIS/ZnS QDs embedded in a polymer matrix. Normalized absorption, emission spectra, and PL decay curves are shown for AIS/ZnS QDs capped with MPA (red) and GSH (blue) after synthesis in water, ligand exchange with OLA/OA in toluene, and embedding in PLMA after polymerization. Reprinted with permission under a Creative Commons CC-BY License from ref. 139. Copyright 2021 The Authors. (e) The two distinct local Au bonding environments in GSH-protected Au NPs corresponding to 600 nm and 810 nm emission, with two amide bonds of GSH omitted for clarity. The absorption, excitation, and emission spectra for the 600 nm- and 810 nm-emitting GSH-protected Au NPs, along with TEM images and core-size distributions for both. Scale bars: 5 nm. Reprinted with permission from ref. 84. Copyright 2016 Wiley.

diffraction and X-ray photoelectron spectroscopy and resulted in a high QY of up to 84%.[115] This improvement is attributed to the passivation effect of the ZnS layer, which reduces surface defects and electronic instability, thereby boosting both the QY and the overall photophysical performance of the QDs. Building on the basic chemistry of Zn^{2+} strongly coordinating with the –COOH group in GSH, this strategy was subsequently applied to coat multinary metal chalcogenide QDs, such as CuInS (CIS) and AIS. These materials have been regarded as safer, greener alternatives or competitors to conventional QDs.[127,141] As shown in Fig. 6b and c, the core–shell design of QDs, with ZnS as the preferred protective shell, significantly reduces surface defects and mediates the band gaps between the inner and outer semiconducting materials. This design results in higher stability, lower toxicity, and enhanced PL performance.[138] As demonstrated in the cases listed in Table 2, QDs with a ZnS shell generally outperform their initial components. Beyond the core–shell structure, the Zn–GSH coordination effect has also been utilized to encapsulate QDs into MOFs, resulting in enhanced antibacterial activity. Zn^{2+} and 2-methylimidazole (2-MeIM), the precursors for ZIF-8, can readily encapsulate quaternary ZAIS QDs. This is facilitated by the strong coordination between Zn^{2+} and both the –COOH group in GSH and the nitrogen atom in 2-MeIM.[82] The use of GSH aligns with the principles of green chemistry in the synthesis of environmentally friendly QDs. This is evident in the comparison of PL properties between ternary AIS/ZnS QDs protected by hydrophobic ligands, such as oleylamine (OLA) and oleic acid (OA), and those protected by GSH (Fig. 6d).[139]

In contrast to the size-dependent emission of QDs, plasmonic MNPs such as Au and Ag display size-independent emission characteristics. As illustrated in Fig. 6e, the local binding geometry of GSH, including factors such as surface coverage and Au–S bond density, significantly influences the emission properties of Au NPs, despite their identical size of approximately 2.6 nm. The multiple functional groups of GSH compensate for the low Au–S density, stabilizing the Au NPs while causing a redshifted emission at 810 nm. As evidenced by circular dichroism (CD) and X-ray absorption, the surface coating by GSH reveals significant effects on the emission properties of Au NPs. Zheng *et al.* leveraged the weakly bonded sites on Au NPs for the production of highly fluorescent Au NPs emitting at 810 nm (rich in Au–O bonds) and dual-emissive Au NPs with peaks at 600 and 810 nm (rich in Au–N bonds).[84] Controlled deprotonation under varying pH conditions, as illustrated in Fig. 2c, activates functional groups in GSH, diversifying surface coating and the corresponding emissions. This process facilitates *in vivo* biological targeting, highlighting GSH's bridging role between the physiological environment and metallic compositions.[60]

3.2 Modulation of charge transfer dynamics

The protecting ligands in luminescent nanomaterials, like GSH, can significantly affect luminescence by facilitating charge transfer to metal cores. This can occur either through metal–sulfur bonding or by directly donating delocalized electrons. These electrons primarily originate from the electron-rich functional groups and atoms present in GSH, further contributing to the stabilization and luminescent properties of the nanomaterials.[142,143] Taking ultra-small Au NPs, namely Au NCs, as a representative, Jin *et al.* studied the HOMO–LUMO gaps of atomically precise $Au_{25}(SR)_{18}$ protected by different ligands, revealing that the abundant electron-rich atoms and functional groups in GSH can significantly enhance the PL of Au NCs, which explained a generally higher QY of biomolecules, like BSA and DNA, than normal thiols.[144] A recent study further investigated the luminescence of $Au_{25}(SR)_{18}$, comparing GSH with three other hydrophobic ligands (phenylethanethiolate, 1-naphthalenethiolate, and selenophenolate). Interestingly, the visible and near-infrared (NIR) emission regime of Au_{25} NCs was attributed to core–shell charge transfer and the Au_{13} inner core, respectively. Consequently, visible emission is more influenced by protecting the surface with different types of ligands, where GSH leads to a blue-shifting emission pattern in the visible light regime (Fig. 7a).[131]

The interest in developing luminescent MNCs extends beyond gold to other noble metals and transition metals. Similarly, the chelating groups and electrostatic stabilization provided by GSH make the synthesis of luminescent Ag, Pt, and Cu NCs manageable, and these NCs exhibit their distinct fluorescence properties as potential probes for bioimaging applications.[38,61,70,103,133]

More interestingly, the concept of AIE can be extended to both Au(I)–SG complexes and GSH-protected Au NCs. By restricting intramolecular rotation and vibration, AIE minimizes the non-radiative decay of the excited electrons, thereby allowing the energy to be released as emission rather than dissipated.[146,147] The Au(I)–SG complexes did not exhibit emission but became highly luminescent when subjected to non-solvent (*e.g.*, ethanol),[95] metal cations (*e.g.*, Zn^{2+} and Cd^{2+}),[148] and spatial confinement (*e.g.*, polymers),[149] and the structural rigidity imposed by aggregation suppresses these motions, leading to a restriction of excited-state relaxation pathways, allowing for efficient radiative recombination. For example, Xie *et al.* investigated nonluminescent oligomeric Au(I)–thiolate complexes and found that these complexes could achieve strong luminescence upon dense aggregation, initiated through either solvent-induced or cation-induced methods (Fig. 7b).[95] Aggregation can bring gold atoms into closer proximity, promoting strong aurophilic interactions.[150] The emission was also found to be heavily dependent on pH, which reflected that the surface charges induced by GSH could affect the degree of aggregation.[151] For example, Luo *et al.* illustrated the mechanism of the pH-switchable interaction among Ag NCs, which is attributed to –COOH groups on the cluster surface that are rich in the citrate and amido functional groups of GSH (Fig. 7c).[145] Following this AIE concept in MNCs, Xie *et al.* further hypothesized that confining the long and interlocked motifs (Au(I)–SG complexes) on the surface of the metallic core could similarly result in enhanced emission. Thus, it was further revealed that the size or length of Au(I) motifs intrinsically influences both the emission energy and the emission pathway of Au NCs. This finding provides valuable insights for the rational design of

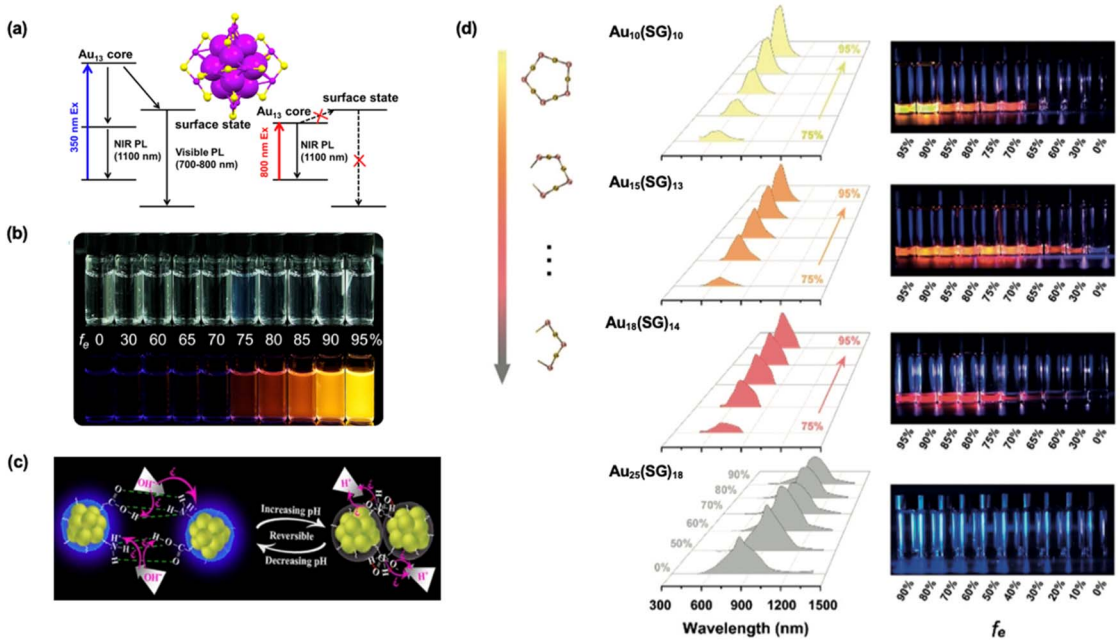

Fig. 7 Charge transfer PL properties of GSH-protected metal nanomaterials. (a) Mechanism of emissions in $Au_{25}(SR)_{18}$. Reprinted with permission from ref. 131. Copyright 2021 American Chemical Society. (b) Digital photos of non-solvent induced AIE Au(I)–thiolate complexes in mixed solvents of ethanol and water with different f_e values under visible (top row) and UV (bottom row) light. Reprinted with permission from ref. 95. Copyright 2012 American Chemical Society. (c) Schematic of the pH-switchable interaction mechanism among the Ag NCs. Reprinted with permission under a Creative Commons CC-BY License from ref. 145. Copyright 2021 The Authors. (d) Illustration of the correlation of emission color with the motifs of Au NCs. Non-solvent induced AIE luminescence spectra with 450 nm excitation (left), and the corresponding digital photos under UV light (375 nm; right) of $Au_{10}(SR)_{10}$, $Au_{15}(SR)_{13}$, $Au_{18}(SR)_{14}$, and $Au_{25}(SR)_{18}$, in the mixed solvent of ethanol and water with different fractions of ethanol. Reprinted with permission from ref. 94. Copyright 2020 Wiley.

highly luminescent MNCs (Fig. 7d).[94] Besides, a strong red emission of $Au_{22}(SG)_{18}$ with a QY of ~8% was reported, though the single-crystal structure of this cluster remains elusive.[128] However, the structure of its alkynyl ligand-protected counterpart reveals a waist band-like hexameric ring of the Au(I)–SG motif, which facilitates strong emission according to the AIE mechanism.[152]

It is remarkable that both the synthetic breakthroughs and AIE concept of MNCs originate from GSH-protected Au NCs, which emphasizes the unique role of the GSH molecule and underscores its potential to guide the development of future highly luminescent species. However, a significant challenge lies in the difficulties associated with achieving monodispersed synthesis and obtaining the single-crystal structures of these nanomaterials. As a result, some advanced PL techniques, including fs-transient adsorption, have found it too complex to directly elucidate the charge transfer dynamics, in contrast to nanomaterials with well-defined structures.

3.3 Chiroptical activity based on ligand chirality

Recently, the intriguing properties of chiral NPs have garnered extensive research attention, driven by their structural similarities to biomaterials and their potential applications in biomedicine.[33,118,119] To impart chiroptical activity to achiral NPs, typical strategies involve the transfer of chirality from chiral ligands. These strategies include (a) decorating achiral NPs with chiral surface molecular ligands, (b) assembling achiral NPs into chiral spatial arrangements, typically induced by chiral molecular linkers, and (c) synthesizing single NPs with chiral morphologies, generally achieved using chiral surface ligands. GSH can participate in all of these strategies, particularly in type (c), where it assists in the construction of complex nanostructures by promoting the formation of chiral morphologies in NPs (Fig. 8a).[153] For example, a recent study reported that GSH can induce active surface growth during the deposition of Au onto Au nanoplates, resulting in the formation of nano-badges with intricate surface patterns (Fig. 8b).[117] A distinctive feature of this growth mode is that the deposition material is directed toward a few active sites, leading to the formation of deep valleys and high-standing walls. The CD signal is influenced by the degree of tilting of the walls, likely originating from the differential packing of chiral ligands on the two pro-chiral slopes. Remarkably, in the absence of templates, chiral gold nanooctopods were directly synthesized using chiral GSH and exhibited chirality-dependent biological responses.

Several factors influence chiral induction in these systems, including GSH concentration, nanomaterial shape,[155] and solvent choice.[156] Conformational changes, weak molecular interactions, and solvent effects-particularly hydrogen bonding-are key in modulating the optical response. Häkkinen *et al.* showed that electronic CD is highly sensitive to solvents, which not only affect the system's optical activity but also form a chiral solvation shell around the nanocluster, enhancing its

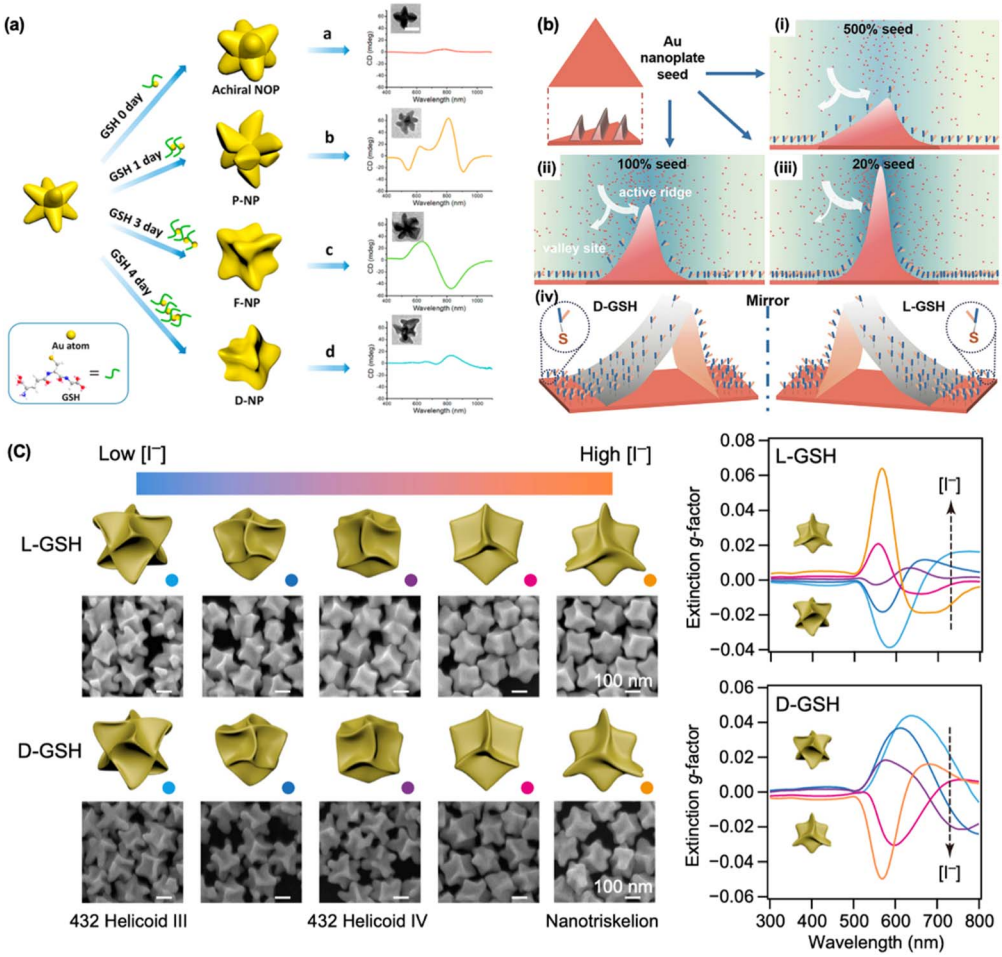

Fig. 8 Chiroptical properties in GSH-protected metal nanomaterials. (a) Schematic representation of the synthesis pathway for Au NPs of distinct morphologies, accompanied by CD spectra illustrating the effects of varying incubation times with L-GSH on the optical properties of the Au NPs. Reprinted with permission from ref. 153. Copyright 2021 American Chemical Society. (b) Schematic illustration of the ridge-valley competition. The triangular nanoplate seed and the side-view show the surface waves/walls. (i–iii) Faster deposition rates increase competition between ridges and valleys, favoring growth on ridge sites. (iv) Chiral ligands are arranged differently on the prochiral slopes, influencing ridge-valley competition and the angles of tilting. Reprinted with permission from ref. 117. Copyright 2023 Wiley. (c) Effect of the KI concentration on the morphology of the obtained chiral nanocrystals and spectral evolution of the extinction *g*-factors for the chiral nanocrystals. Reprinted with permission from ref. 154. Copyright 2023 Springer Nature.

chiroptical properties. In addition, the shape of the nanostructures plays a crucial role in chiral induction. Markovich *et al.* explored the behavior of chiral GSH molecules with silver surfaces and optimized the geometry of gold@silver nanostructures for enhanced near-UV plasmonic CD responses by modulating the coupling between chiral molecules and plasmonic fields.[155] Wang *et al.* also demonstrated that manipulating the directional growth rate of nanostructures can generate a variety of chiral morphologies when homochiral ligands are present.[154] This approach enables the precise control of nanostructure morphology, directly impacting their chiroptical properties (Fig. 8c).

While chirality transfer remains relevant in the field of MNCs, these atomically precise MNCs can possess intrinsic chirality due to the specific arrangement of their metallic core and the protective motifs surrounding them. Chirality in MNCs was detected more than 20 years ago, who worked on MNCs with 20–40 Au atoms protected by L-GSH.[156] The current perspective classifies chirality in MNCs as either intrinsic or induced. Intrinsic chirality arises when the metal core itself is chiral or when there is a chiral arrangement of achiral protective ligands. In contrast, induced chirality occurs when chiral ligands impose chirality onto the metal architecture, like what is observed in NPs. Many MNCs have been reported to exhibit chiroptical activity, either intrinsically or through chiral assembly. However, it is notable that GSH may not be preferred as a ligand in this context due to the challenges associated with obtaining well-defined structures. An intriguing case study involves the chiroptical response of $Au_{25}(SG)_{18}$, whose metallic core is spherically symmetric.[156] Simulations revealed that CD peaks can derive up to 50% of their intensity from transitions involving electronic states of the solvation shell, which adopts a chiral arrangement around the organic thiol-protected surface.

3.4 Available conjugation sites for tunable emissions

Notably, the multiple functional groups of GSH offer an opportunity to further regulate the luminescence by interacting with the exterior environment (*e.g.*, solvents, molecules, and cells). It is well established that GSH-protected QDs can be recognized by various biomolecules, including proteins, DNA, and cells. Furthermore, the conjugation of these QDs with biomolecules also influences their PL properties. DNA-directed self-assembly of 3-mercaptopropionic acid (MPA) and GSH-protected QDs exhibited infrared emission, demonstrating potential as a tissue imaging agent.[120] Besides, based on PL variation, GSH-protected QDs are also frequently designed as chemical sensors for the quantitative detection of toxic metal ions, such as Hg^{2+} and Pb^{2+}.[157,158] This is also evidenced by the enhanced CD performance of chiral GSH-protected Cu NCs by covalently bonding with Co^{2+}. More interestingly, GSH-protected QDs can be conjugated with dye molecules, leading to fluorescence resonance energy transfer (FRET) and/or charge

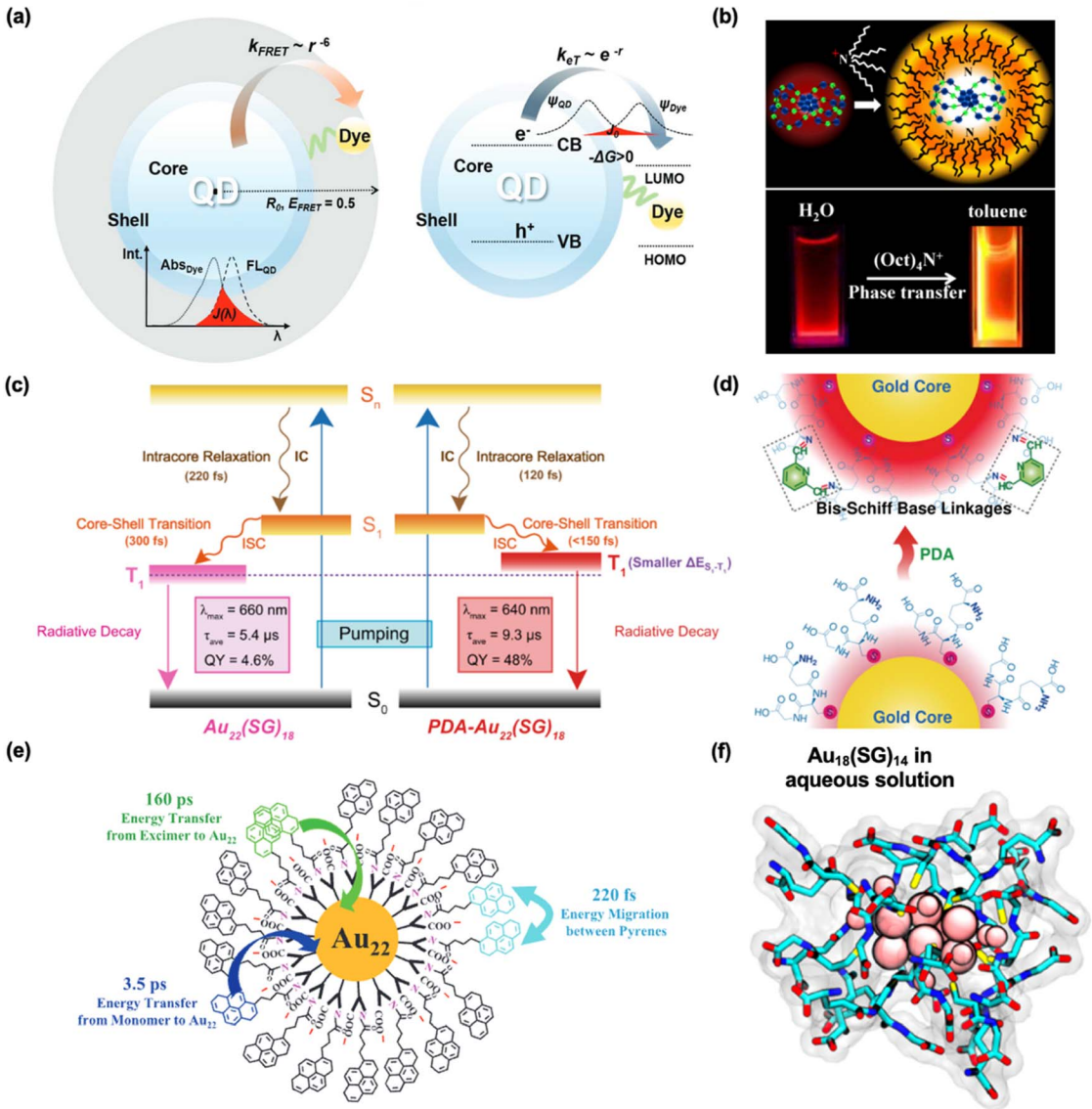

Fig. 9 Roles of conjugation in the PL of GSH-protected metal nanomaterials. (a) A FRET construct consisting of a QD and a dye, where the Förster distance (R_0) is measured from the center of the QD, indicating the effectiveness of FRET. Reprinted with permission from ref. 46. Copyright 2018 Wiley. (b) A scheme showing the binding of TOA to $Au_{22}(SG)_{18}$ (Au, blue; S, green). A digital photograph of $Au_{22}(SG)_{18}$ in water and TOA-Au_{22} clusters in toluene under long-wavelength UV lamp irradiation (365 nm). Reprinted with permission from ref. 129. Copyright 2015 American Chemical Society. (c) Schematic diagram illustrating the excited-state dynamics of $Au_{22}(SG)_{18}$ and PDA-$Au_{22}(SG)_{18}$ NCs. (d) A schematic showing the correlation between emission intensity and PDA binding on the $Au_{22}(SG)_{18}$ surface. PDA binding induces intramolecular ligand cross-linking through bis-Schiff linkages, resulting in enhanced PL. Red shading indicates the PL intensities of $Au_{22}(SG)_{18}$ before and after PDA addition. Reprinted with permission under a Creative Commons CC-BY License from ref. 130. Copyright 2022 The Authors. (e) Schematic diagram illustrating energy migration and energy transfer processes taking place in $Au_{22}(SR)_{18}$. Reprinted with permission from ref. 159. Copyright 2021 Wiley. (f) Simulated ligand configuration of $Au_{18}(SG)_{14}$ in aqueous solution showing the numerous available conjugation sites, which is supported by EXAFS analysis. Reprinted with permission from ref. 32. Copyright 2018 American Chemical Society.

transfer processes, which have promising biosensing and PDT applications (Fig. 9a).[46]

GSH-protected MNCs also benefit from ligand conjugation, which enhances their emission properties. Of particular interest, the surface dynamics of $Au_{18}(SG)_{14}$ are currently being investigated and compared to those of its cyclohexanethiolate-protected counterpart in solution using extended X-ray absorption fine structure (EXAFS) analysis (Fig. 9f).[32] GSH encapsulates the metallic core through intermolecular interactions arising from its various functional groups, effectively minimizing structural changes induced by interactions with water molecules. This encapsulation underscores the rigidified surfaces of GSH-protected nanomaterials and highlights the numerous available conjugation sites provided by the functional groups.

For instance, the QY of $Au_{22}(SG)_{18}$ could be further enhanced by up to 60% by a shell rigidification strategy with the bulky tetraoctylammonium cations (Fig. 9b).[129] As shown in Fig. 9e, the same group developed an efficient amide coupling strategy by conjugating red-emissive $Au_{22}(SG)_{18}$ with light-absorbing chromophores, which can lead to unique triple-emission gold-based nanocomposites.[159] More recently, bis-Schiff base linkages were utilized to restrict intramolecular motion by crosslinking 2,6-pyridinedicarboxaldehyde (PDA) with the surface of $Au_{22}(SG)_{18}$.[130] The resulting high emission efficiency was attributed to the PDA-induced crosslinking, which enhances the rigidity of the surface-bound Au(I)–SG motifs (Fig. 9c and d). Additionally, GSH-protected MNCs can be confined within NaCl crystals, which enhances their emission and improves photostability. A combination of NaCl-confined Au NCs and Cu NCs has been shown to generate white light-emitting devices.[160] Further designs for enhanced and tunable emissions of GSH-protected MNCs are anticipated through interactions with the external environment.

4. Theranostic applications of GSH-protected metal nanomaterials

GSH-protected metal nanomaterials represent a distinctive class of theranostic agents, effectively combining therapeutic and diagnostic functionalities within a single platform. In this "Inseparable Duo", on the one hand, GSH occupies a pivotal position at the bio–nano interface, playing a crucial role in modulating bio–nano interactions by imparting biocompatibility, stability, and surface recognition properties.[161,162] On the other hand, the metallic component contributes a range of functionalities, including photothermal and photodynamic effects, and provides contrast in imaging applications, making the duo highly effective in theranostic uses.[43,163] Specifically, the GSH ligand shell ensures a non-toxic, biologically friendly interface while enhancing the permeability and retention (EPR) of the metal core. This combination enables the nanomaterials to effectively carry out a range of biological tasks with improved efficiency and safety.[164] In cancer therapies, GSH has an isoelectric point (~6) similar to the pH of tumor cells, making GSH-protected metal nanomaterials more pH-responsive in acidic tumor environments.[37] Remarkably, GSH-protected nanomaterials show particular promise in liver tumor treatment. The highly exposed GSH on the surface can activate GSH transporters within liver cells,[165] facilitating the uptake of these nanomaterials by liver cancer cells. This enhances the accumulation of the nanomaterials inside the tumor, potentially improving the efficacy of the treatment.

Generally, the theranostic functionalities of GSH-protected nanomaterials are intrinsically linked to their decay behaviors following excitation. The most common excitation source is light, after which the excited nanomaterials follow preferred pathways to return to their ground states.[48] Thus, radiative decay manifests as PL, leading to applications in bio-sensing and bio-imaging. Conversely, a prevalent form of non-radiative decay involves the generation of heat, a phenomenon that can be effectively utilized in PTT. Materials exhibiting strong absorption in the NIR region undergo rapid heating upon light irradiation, thereby creating hyperthermic conditions that promote tumor cell apoptosis through mechanisms such as protein denaturation, membrane disruption, and DNA damage,[43] and magnetic hyperthermia therapy (MHT)[166] if magnetic NPs are involved. Additionally, some nanomaterials can return to their ground states through chemical pathways, producing ROS in the process,[167] which is utilized in PDT. ROS play a crucial role in cancer treatment by inducing oxidative stress, thereby promoting the selective destruction of cancer cells.[47] Similar mechanisms occur when excitation sources extend beyond light to other electromagnetic waves, such as X-rays. GSH-protected metal nanomaterials can also function as radiosensitizers in RT.[49]

Therefore, it is crucial to first address concerns about the biosafety of GSH-protected metal nanomaterials, which is of paramount importance. This biosafety can be attributed to the intrinsic biocompatibility, zwitterionic nature, and chirality of GSH.[168] Then, we aim to highlight several major theranostic applications, including bio-sensing, bio-imaging, and anti-cancer bio-therapies, that highlight the synergistic effects of this "Inseparable Duo".

4.1 Evaluation of biocompatibility and biosafety

The biocompatibility and biosafety of GSH-protected metal nanomaterials are critical considerations before delving into their biomedical applications. First and foremost, GSH is water-soluble and inherently biocompatible. Zheng *et al.* carried out a systematic study on the pharmacokinetics of GSH-protected Au NPs.[169,170] The presence of GSH on the surface of these nanomaterials has been shown to mitigate cytotoxicity by minimizing oxidative stress, thus enhancing their biocompatibility. For example, GSH-protected Au NPs showed a rapid distribution to and rapid clearance from the skin compared to dyes (Fig. 10a).[171] In comparison to Au NPs protected by other ligands, such as cetyltrimethylammonium,[173] GSH-protected Au NPs demonstrated superior stability under physiological pH conditions, greater stealthiness towards reticuloendothelial tissues, and a faster renal clearance rate.[165,174,175] Smaller nanoparticles tend to be excreted *via* the kidneys through urine.

Notably, the GSH coating on metal nanomaterials plays a crucial role in their biocompatibility by preventing aggregation and reducing the potential for long-term accumulation in organs, ultimately minimizing toxicity. For detailed drug delivery systems, their absorption, distribution, metabolism, and excretion *in vivo* present complex challenges that influence their efficacy and safety (Fig. 10d).[172,176] The absorption of NCs is impacted by their size, surface charge, and administration route, with smaller particles being more effective for intravenous delivery. Upon entering the bloodstream, NCs are

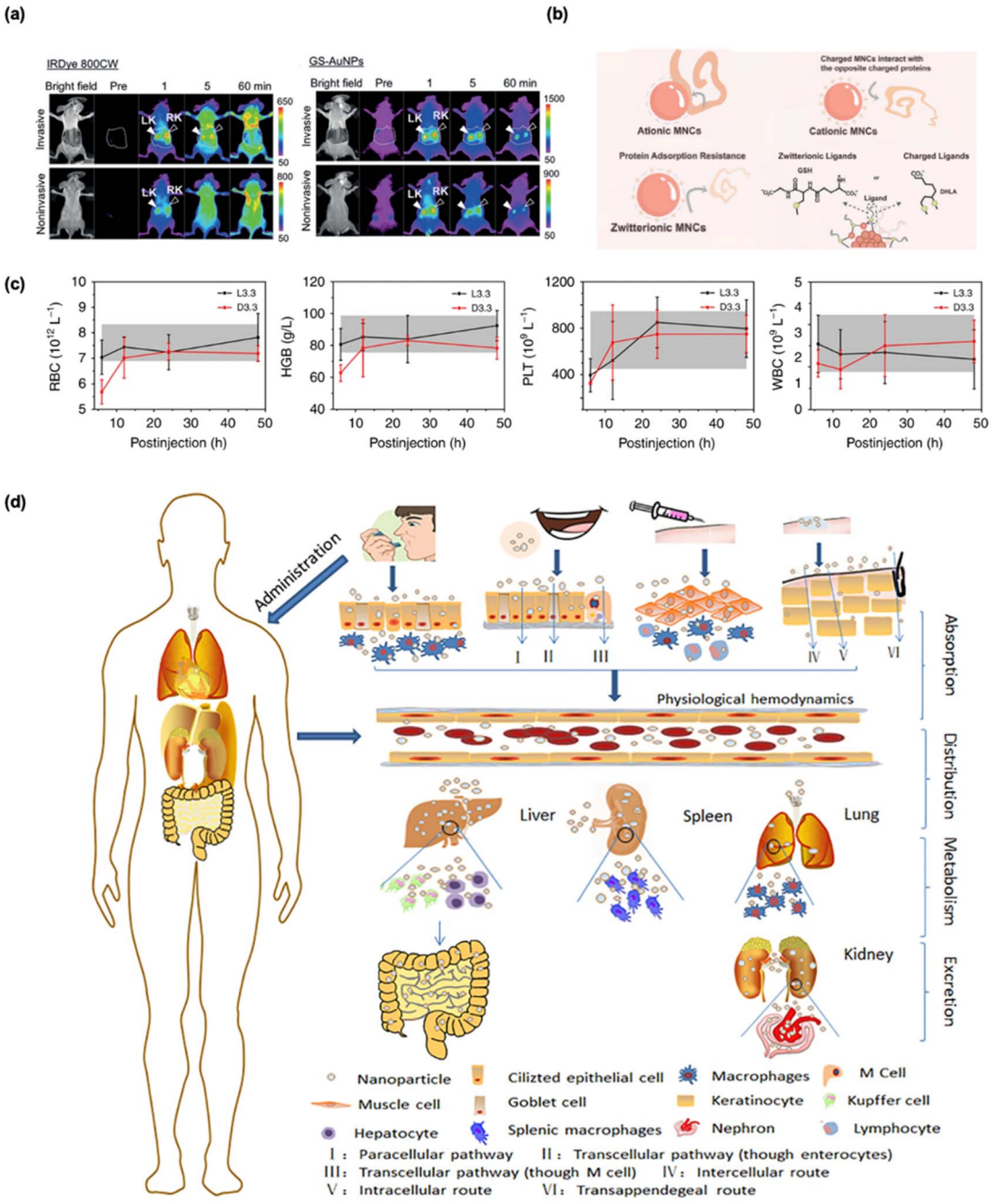

Fig. 10 Evaluation of the biocompatibility and biosafety of GSH-protected metal nanomaterials. (a) Comparison of renal-clearable NIR-emitting IRDye 800CW and renal-clearable NIR-emitting GSH-protected Au NPs by *in vivo* fluorescence kidney imaging. Reprinted with permission from ref. 171. Copyright 2019 Wiley. (b) Examples of thiolate ligands for MNC surface modification and surface charge influence on protein adsorption onto MNCs. Readapted with permission from ref. 162. Copyright 2024 Wiley. (c) Hematological parameters (red blood cells, hemoglobin, platelets, and white blood cells) in mice following L3.3 or D3.3 treatment at 6, 12, 24, and 48 hours and return to the normal range in a short time after postinjection. Shaded areas denote normal control ranges. Reprinted with permission under a Creative Commons CC-BY License from ref. 22. Copyright 2020 The Authors. (d) Scheme of absorption, distribution, metabolism, and excretion of nanomaterials *in vivo*. Reprinted with permission from ref. 172. Copyright 2020 Elsevier.

distributed to organs like the liver and spleen, where their accumulation depends on factors such as size and the mononuclear phagocytic system.[177] Metabolism involves the degradation of NCs, releasing their drug payload either through enzymatic processes or pH-sensitive hydrolysis, with organic nanoparticles typically being more biodegradable than inorganic ones. Excretion occurs mainly *via* the liver or kidneys, with smaller particles (<5 nm) being cleared through renal filtration and larger ones *via* hepatobiliary pathways. The physicochemical properties of NCs, including size, shape, and surface modifications, are crucial for optimization, enhancing targeted delivery while minimizing toxicity.[178] Also, the same group investigated the relationship between GSH-protected Au NP size and renal clearance efficiency, revealing that the glomerulus functions not as a simple "size-cutoff" filter but as an atomically precise "bandpass" barrier, significantly slowing the renal clearance of ultrasmall Au NPs in the sub-nanometer range.[179] Furthermore, the tumor microenvironment, characterized by leaky vasculature and poor lymphatic drainage, differs significantly from normal tissues and can facilitate the accumulation of certain types of drugs.[180–184] This phenomenon is known as the enhanced EPR effect and is observed in GSH-protected Au NPs compared to the small dye molecules.[169]

Under psychological conditions, the γ-glutamyl group in GSH would carry one positive and one negative charge simultaneously, making it a zwitterionic ligand. The concept of employing zwitterions for enhanced biocompatibility and stability in nanomaterials was introduced as early as 2007.[185] The coupling of four ligands, namely dihydrolipoic acid, cysteamine, cysteine, and dihydrolipoic acid, with PEG, was tested for their blood clearance and body distribution when assembled onto the surface of QDs. The study concluded that NPs protected by zwitterionic ligands were less likely to be adsorbed by serum proteins, resulting in faster clearance from the body and reduced toxicity. For instance, Zheng *et al.* studied GSH-protected Au NCs with high resistance to serum protein adsorption, as shown in Fig. 10b, demonstrating that these surface ligands enhance physiological stability and reduce protein adsorption.[162,186] This improvement enables more accurate coordination of preoperative planning and surgery, potentially increasing the effectiveness of radical resection. Therefore, GSH-protected nanomaterials are frequently regarded as promising biosafe candidates for various biomedical research applications, including anti-cancer therapy.[187] As a zwitterionic surface ligand, GSH often outperforms other hydrophilic modifications, such as PEG. GSH's unique ability to facilitate the EPR effect ensures that these NPs accumulate more efficiently in tumor tissues, improving their targeted delivery.[185] Simultaneously, GSH lowers cytotoxicity and enhances overall therapeutic outcomes, due to its natural occurrence and ease of metabolism.[174] This allows for safer and more efficient clearance[179] of GSH-protected nanomaterials, reducing the risk of accumulation-related toxicity and making them more favorable for long-term biomedical applications.

Another critical consideration is the chirality of nanomaterials.[118] Biological systems exhibit high selectivity, preferring L-amino acids and D-sugars, which makes chirality an essential factor for designing safe and effective nanomedicines. This specificity is critical when developing GSH-protected metal nanomaterials for therapeutic applications. A mismatch in chirality, as illustrated by the case of thalidomide's enantiomers-where (*R*)-thalidomide acts as a sedative but (*S*)-thalidomide causes teratogenic effects-highlights the importance of careful design to ensure non-toxicity and prevent adverse effects.[188,189] For example, Tang *et al.* evaluated the biosafety of both L-GSH and D-GSH (Fig. 10c). The results indicated that hematological parameters experienced slight fluctuations at the early stages post-injection, subsequently returning to normal ranges, thereby demonstrating favorable biosafety profiles.[22] Beyond effectiveness, the chirality of GSH might even affect the biocompatibility of the nanomaterials.[189,190] The effect of chirality by using L-GSH or D-GSH coated CdTe QDs has been investigated. By keeping other variables identical, such as the size of QDs, it was observed that L-GSH-protected QDs were more likely to induce autophagy, resulting in a greater extent of cell death. Similar scenarios can also be found in the cellular intake difference in chirality of different Au NPs.

4.2 Bio-sensing

GSH not only serves as a protective ligand but also plays a critical role in bio-sensing by facilitating interactions with various analytes. One notable example is its interaction with GST, an enzyme overexpressed in certain cancer cells, which provides a potential pathway for cancer diagnostics. GSH also plays a crucial role in sensing oxidative stress. Its thiol groups can form –S–S– under oxidative conditions, which alters the properties of the nanomaterial. This change can be exploited to detect oxidative stress in biological systems. This redox-responsive behavior makes GSH-protected metal nanomaterials promising candidates for oxidative stress sensing and tumor cell detection.[24] Their ability to respond to changes in oxidative pressure could be harnessed for targeted diagnostics.

Owing to the unique interactions between GSH and specific analytes,[191] bio-sensing can be achieved using GSH-protected nanomaterials. GSH, located on the surface of these nanomaterials, is the first point of contact with external molecules (analytes). Zheng *et al.* demonstrated ultra-small Au NCs as an effective fluorescent probe and blood marker for noninvasive monitoring of hepatic GSH depletion and recovery in drug-induced liver injury (Fig. 11a). The dye indocyanine green (ICG) conjugated to GSH-protected Au NCs showed high specificity, efficient clearance, and minimal nonspecific accumulation, supporting their potential for clinical translation.[39] A prime example of this bio-sensing capability is the strong interaction between GSH and the enzyme GST. An assembly between GSH-protected Au NCs and cysteamine-protected Au nanorods (NRs) was designed.[192] The authors reported a FRET in this conjugation, where energy is transferred from a donor to an acceptor due to their close proximity. In this case, GSH-protected Au NCs were bound to Au NRs through electrostatic interaction between GSH and cysteamine. When fluorescent Au NCs were excited by light, they transferred energy to the NRs instead of exhibiting emissions. However, in the presence of

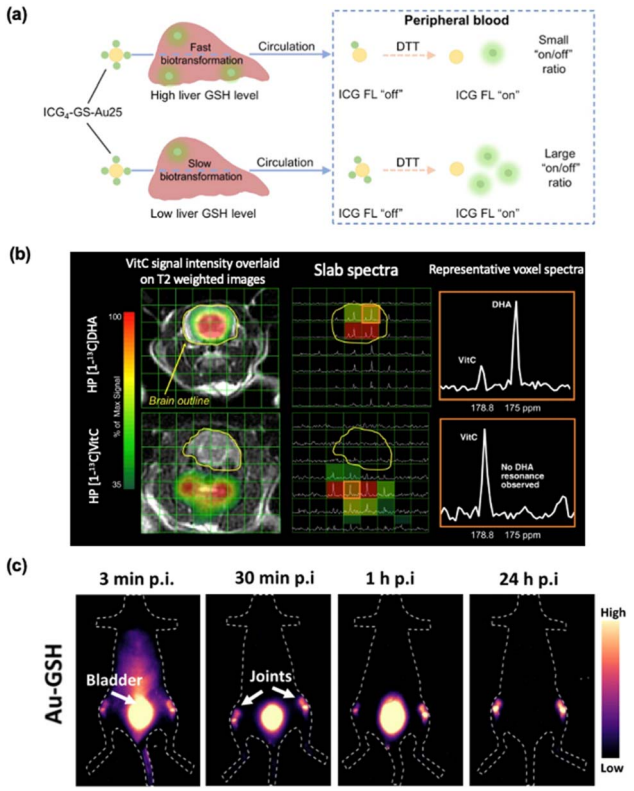

Fig. 11 Bio-sensing and bio-imaging applications of GSH-protected metal nanomaterials. (a) Schematic of the rationale for a blood sampling-based detection method using ICG_4-GSH-protected Au_{25}. Reprinted with permission under a Creative Commons CC-BY-NC 4.0 License from ref. 39. Copyright 2021 The Authors. (b) 2D chemical shift imaging with hyperpolarized ^{13}C ascorbates reveals different transport and compartmentalization of dehydroascorbate and vitamin C based on GSH content detection. Reprinted with permission under a Creative Commons CC-BY License from ref. 12. Copyright 2018 The Authors. (c) *In vivo* fluorescence imaging with intravenous injected GSH-protected Au NCs. Reprinted with permission under a Creative Commons CC-BY License from ref. 188. Copyright 2022 The Authors.

GST, the assembly between Au NCs and Au NRs would disassemble due to the stronger interaction between GSH and GST. Au NCs would recover their fluorescent intensity, indicating the presence of GST. Building on this concept, the group also adopted a similar strategy of FRET between GSH-protected Mn-doped ZnS QDs and graphene oxide, successfully extended to other biological samples.[15]

Another intriguing application of GSH-protected nanomaterials is their use in detecting inflammation. Inflammatory reactions, a common pathophysiological process in many diseases, lead to the overproduction of ROS. Thus, a ROS-responsive cross-linking strategy is reported for the *in vivo* detection of inflamed areas using GSH-protected LNPs in the NIR-II region. In this system, the two –COOH groups in GSH coordinate with lanthanide cations, while the thiol group can be oxidized by ROS to form a –S–S–. Thus, ROS-responsive cross-linking between GSH-protected nanomaterials can be realized specifically at the inflamed area. This cross-linking facilitates the enhanced accumulation of nanoprobes within inflamed regions by increasing the particle size, thereby reducing the excretion rate and prolonging retention in the target area.

4.3 Bio-imaging

In general, real-time bio-imaging at the cellular, subcellular, and molecular levels is crucial for the early detection and treatment of life-threatening diseases such as cancer. GSH-protected nanomaterials present substantial potential for bio-imaging applications owing to their tunable optical properties. GSH's capacity to modulate surface properties can significantly enhance PL, rendering these nanomaterials ideal candidates for bio-imaging techniques.[193–195] Additionally, GSH-protected metal nanomaterials serve as versatile contrast agents across various imaging modalities, including optical imaging under visible or NIR light for visualizing biological samples, magnetic resonance imaging[12] using magnetic fields and radio waves for detailed soft tissue visualization, and computed tomography (CT)[170] with X-rays for generating cross-sectional images. As shown in Fig. 11b, Wilson *et al.* utilized ^{13}C magnetic resonance spectroscopy as a mapping probe, implementing this imaging technique on normal rat brains and in a rat model with GSH depletion.[12] These capabilities enable more precise and accurate diagnostic assessments in biomedical contexts.

GSH can enhance the water solubility and biocompatibility of QDs without markedly compromising their PL properties. This improvement renders GSH-protected QDs suitable candidates for various bio-imaging applications. As an approach for early kidney disease detection, Zheng *et al.* applied photoacoustic imaging to track the *in situ* transport of GSH-protected Au NCs from the aorta into the renal parenchyma.[196] Zheng *et al.* developed a GSH-protected fluorescent gold nanoprobe capable of binding to serum proteins and being transported to the liver. This enabled the non-invasive imaging of biotransformation kinetics *in vivo* with high specificity, allowing examination of the process at a chemical level.[197] Ying *et al.* developed GSH-protected CdTe QDs and tried out its cell imaging application.[9] Due to its small size and the capacity of GSH to bioconjugate with other molecules, this nanomaterial can be effectively utilized for the staining of subcellular organelles. For instance, after conjugation with biotin, GSH-protected CdTe QDs were successfully used to label the cytoskeleton. The great potential of GSH as a ligand is further demonstrated in another study by Ying *et al.*[79] As a tripeptide, GSH on the surface of NPs can engage in intermolecular interactions, facilitating the formation of amide bonds between adjacent GSH molecules. This intraparticle cross-linking was effectively demonstrated in GSH-protected CdTe QDs, leading to the creation of a protective coating around the NPs.

Moreover, numerous GSH-protected nanomaterials exhibit high QY in the NIR region. This NIR PL property is advantageous as it minimizes tissue absorption, thereby enhancing imaging depth and providing high spatial resolution. The PL properties combined with the low cytotoxicity of GSH-protected nanomaterials position them as excellent candidates for bio-imaging applications.[7,8,175,198,199] For instance, Dai *et al.*

investigated subcutaneous injection of Au NCs, demonstrating that this approach enables lymph node mapping *via* NIR-II fluorescence imaging, with an optimal visualization window occurring approximately 0.5–1 hour post-injection, followed by efficient renal clearance (Fig. 11c).[188] Moreover, Luo *et al.* successfully synthesized $Ag_{14}(SG)_{11}$ and further investigated its efficacy for cell imaging. Their findings indicated that this GSH-protected nanomaterial was internalized by the cells while exhibiting minimal cytotoxicity. Notably, Ag_{14} demonstrated superior stability compared to small organic molecules, such as Hochst 33342 and acridine orange. The PL intensity of Ag_{14} remained consistent even after photobleaching for over one hour, underscoring their robustness for applications in bio-imaging.[8] In addition to cell imaging, *in vivo* imaging is also achieved with GSH-protected nanomaterials. Imaging of kidney clearance kinetics was achieved with GSH-protected Au NPs, which have a better performance compared to conventional NIR dyes.[175]

4.4 Bio-therapies

GSH-protected metal nanomaterials hold significant promise in biotherapy, showing potential for application in a range of diseases, including Alzheimer's[191] and Parkinson's.[17] Notably, their unique properties make them particularly effective in cancer therapy, which remains our primary focus. GSH-protected metal nanomaterials have demonstrated significant promise in PTT and PDT, where their ability to absorb light and convert it into heat or ROS can selectively kill cancer cells.[166] The biocompatibility of GSH ensures minimal side effects during these therapies, enhancing patient safety.[183] Moreover, GSH-protected metal nanomaterials have potential applications in RT as radiosensitizers, enhancing the effectiveness of radiation treatment.[48] Magnetic metal nanomaterials functionalized with GSH can also be utilized in MHT, where their magnetic properties are exploited to generate localized heating for tumor ablation, offering another avenue for cancer treatment. The integration of various therapeutic modalities in combined treatment regimens presents significant potential for improving overall therapeutic efficacy and patient outcomes in cancer treatment.

In PTT, the temperatures of targeted cancer cells are elevated in the range of 40–45 °C, causing protein denaturation and ultimately cell death. It has a more toxic impact on cancer disease, where many studies declared that cancer tissue is more sensitive to heat injury than normal tissue. The development of GSH-protected metal nanomaterials now enables more control of the thermal energy delivered to the tumor region. Furthermore, Zheng *et al.* employed GSH-protected Au NCs as a dye-delivery vector, achieving improved photochemical stability, enhanced photothermal performance, prolonged blood circulation, and increased tumor-targeting specificity (Fig. 12a). These attributes collectively contributed to significantly enhanced efficacy in PTT.[200] Moreover, Jiang *et al.* synthesized gold–silver nanocages with tumor-targeted properties, which demonstrated effective PTT capabilities for cancer treatment.[202] Furthermore, Li *et al.* explored PTT of $Au_{25}(SG)_{18}$ for the MDA-MB-231 breast cancer cells, demonstrating significant photothermal activity that resulted in 100% cell death upon laser excitation. This finding suggests that Au NCs could have

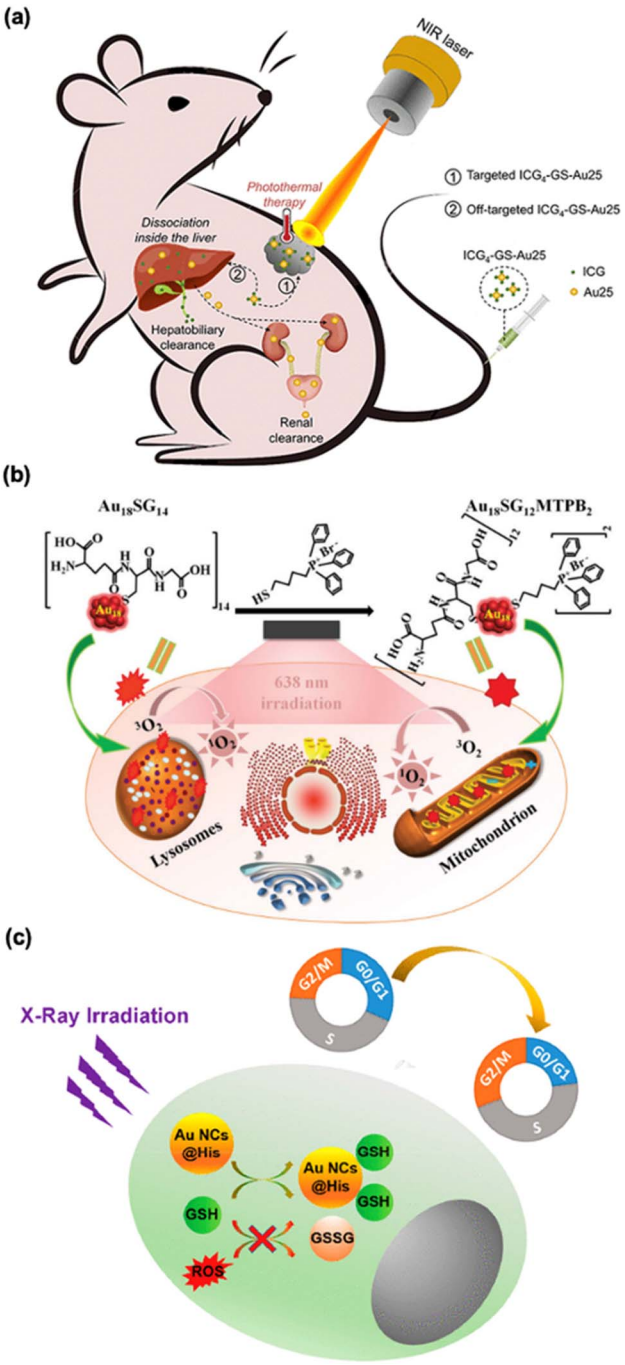

Fig. 12 Representative anti-cancer bio-therapies of GSH-protected metal nanomaterials. (a) GSH-protected Au_{25} NCs mediate PTT and subsequent *in vivo* clearance pathways. Reprinted with permission from ref. 200. Copyright 2020 American Chemical Society. (b) Synthesis of $Au_{18}(SG)_{12}(MTPB)_2$ and its switching of intracellular targeting organelles and PDT toward cancer cells. Reprinted with permission from ref. 201. Copyright 2018 Royal Society of Chemistry. (c) Schematic illustration of the RT therapeutic principle based on GSH-protected Au NCs. Reprinted with permission from ref. 50. Copyright 2018 American Chemical Society.

expanded applications in PTT for major illnesses.[105] It should be noted that radiative decay and non-radiative decay are competing after excitation. Therefore, potential candidates for PTT should not be highly emissive, thus excluding most QDs and LNPs. Several PTT cases have been reported in Au NPs, and now research interest has extended to ultrasmall Au NCs.

Converting $^3O_2$ to highly reactive singlet oxygen $^1O_2$ is essential for cancer treatment *via* utilizing PDT. In 2014, Jin *et al.* first reported that $Au_{25}(SG)_{18}$ showed superior biocompatibility and photodynamic activity against the cancer cells.[47] The results demonstrated that singlet oxygen $^1O_2$ could be effectively obtained *via* direct photosensitization for $Au_{25}(SG)_{18}$ under NIR photoexcitation, which was important for the Au NCs in photodynamic applications. Zhu *et al.* revealed that $Au_{18}(SG)_{14}$ was accumulated at the lysosome sites as shown in Fig. 12b, while $Au_{18}(SG)_{12}(MTPB)_2$ (MTPB = (4-mercaptobutyl) triphenylphosphonium bromide) tended to concentrate in the mitochondrial sites to enable the target switching.[201] Likewise, it was shown that $^1O_2$ was formed by these two Au_{18} under photoexcitation at 638 nm. Moreover, it was demonstrated that $Au_{18}(SG)_{12}(MTPB)_2$ with a lower amount of $^1O_2$ exhibited the same biotoxicity for cancer cells compared with $Au_{18}(SG)_{14}$, which indicated superior photodynamic activity at mitochondrial sites for killing cancer cells than that at the lysosomal sites. Moreover, Bohidar *et al.* investigated AIS QDs and examined their potential as carriers for photosensitizers, highlighting their applicability in cancer diagnosis and PDT.[203]

In addition, Xie *et al.* reported two new kinds of radiosensitizers, including $Au_{25}(SG)_{18}$ and BSA-Au_{25} NCs for RT, in which $Au_{25}(SG)_{18}$ was intended to accumulate in the tumors and in turn exhibited more excellent enhancement for cancer treatment compared with BSA-Au_{25} and large Au NPs, highlighting that the size and structure of the coating ligand play a crucial role in determining the efficiency of cancer RT.[204] Moreover, Wu *et al.* developed a straightforward synthesis of GSH-protected Au NCs, presenting a novel strategy for designing radiosensitizers. These NCs effectively reduce intracellular GSH levels, thereby minimizing the depletion of generated ROS by GSH, enhancing therapeutic efficacy (Fig. 12c).[50] Furthermore, Xie *et al.* first explored the potential of $Au_{10-12}(SG)_{10-12}$ as radiosensitizers for consuming tumors and for cancer RT in mice grafted with a human cervical U14 tumor.[205] The GSH shell facilitated this by reducing the absorption of Au NCs by non-target tissues and promoting the activation of transporters on the tumor cell surface.[17]

5. Conclusions and outlook

In this *perspective*, we reviewed the multifaceted impact of GSH on the synthesis, PL properties, and nanobiomedical applications of metal nanomaterials. Through a discussion of various scales of metal nanomaterials, from atomically precise MNCs to MNPs, QDs, and LNPs, we emphasize the pivotal role of GSH. Its diverse roles, ranging from stabilizing metal nanomaterials to enhancing biocompatibility and bio–nano interactions, were highlighted. The roles of GSH are summarized in the general synthesis strategies for metal nanomaterials, namely protecting ligands, dual roles in the Brust–Schiffrin method, surface etching, and GSH-mediated ligand exchange reactions. Then, the PL properties of GSH-protected metal nanomaterials are discussed, where GSH is actively involved in the surface coating of nanocrystals, modulation of the charge transfer of MNCs, inducing chiroptical activities, and providing conjugation sites with external molecules. Last, this *perspective* also highlights the "Inseparable Duo" of GSH and the metallic core it protects by showcasing some important biomedical applications, such as bio-sensing, bio-imaging, and anti-cancer bio-therapies including PTT, PDT, and RT. Hereafter, we would also like to provide several interesting perspectives on the future development of GSH-protected metal nanomaterials.

5.1 Smart synthesis-assisted designs of new probes

The development of GSH-protected metal nanomaterials has been revolutionized by smart synthesis, leveraging data-driven techniques, automation, and AI to optimize synthesis parameters.[206,207] This approach has facilitated the rapid and precise design of nanoprobes tailored for specific PL properties and biomedical applications. A recent breakthrough utilized PL spectra as efficient markers for correlating synthesis recipes with PL properties in GSH-protected Au NCs.[91] A trained extreme gradient boosting model helped elucidate relationships between synthesis variables and QYs, setting a foundation for future design optimizations. A proposed closed-loop workflow for smart synthesis consists of data mining, automated design, synthesis, analysis, and feedback. Advances in robotic synthesis and data-driven optimization further enhance this paradigm, making scalable, adaptive synthesis of high-performance GSH-protected nanoprobes increasingly achievable.[208]

5.2 Precise structure-to-property relationships

Advancing GSH-protected metal nanomaterials requires an in-depth understanding of structure-to-property relationships. Historically, GSH has greatly facilitated MNC synthesis due to its protective capabilities, yet the "GSH dilemma" persists due to challenges in atomic-level structure determination, which led to a shift toward alternative ligands for crystallization. The resulting lack of structural clarity hinders insights into how specific structural features (core configuration and ligand orientation) affect optical, electronic, and catalytic properties, as exemplified by the unclear emission origin in $Au_{22}(SG)_{18}$.[26] Emerging techniques like SANS[209] and EXAFS[32] now enable detailed characterization of GSH-protected structures, advancing the understanding of metal–ligand interactions and enabling the rational design of MNCs with tailored functionalities.

5.3 *In vivo* synthesis within biological systems

In vivo synthesis within biological systems offers a novel approach for creating metal nanostructures directly within living organisms. GSH, with its thiol-rich cysteine residue, is instrumental in forming metal–sulfur bonds with metals such as Au and Ag, acting as a reducing agent, protective ligand, or

synthesis mediator. This biocompatible, sustainable method integrates with cellular processes and enhances nanomaterial functionality in biomedical applications. Notable examples include bacterial synthesis of metal nanostructures and therapeutic applications, where engineered bacteria target tumors to produce ROS-generating FeS NPs.[164,210] Overexpression of GSH in cancer cells also facilitates intracellular synthesis of fluorescent probes, advancing prospects in nanomedicine.[187,211,212] As understanding of these biosynthetic mechanisms grows, *in vivo* synthesis is likely to broaden applications in medicine, environmental sensing, and catalysis.[174]

5.4 Diverse applications of GSH-protected metal nanomaterials

GSH-protected metal nanomaterials have a broad range of applications beyond biomedicine, showing promise in energy, catalysis, nanozymes, and environmental remediation. The versatile chemistry of GSH as a ligand enables tunable properties, making these nanomaterials highly adaptable across different fields.

In energy applications, GSH-protected nanomaterials, such as Au NCs and QDs, are effective as photosensitizers in hydrogen production and photocatalysis.[160,213] For example, GSH-protected CdSe QDs, combined with a cobalt precatalyst, have demonstrated substantial hydrogen yields.[214] Additionally, the coating of PbS QDs with GSH is expected to lead to longer exciton lifetime in the QDs and improved charge injection from PbS QDs into the conduction band of TiO_2.[72] For photocatalysis, GSH-protected metal nanomaterials are effective in reactions like water splitting,[215] and CO_2 reduction, stabilizing NPs in aqueous media while boosting interaction with reactants.[216] These materials leverage GSH's biocompatibility, supporting green energy solutions and environmental cleanup.

In catalytic applications, Lei *et al.* developed a strategy for fabricating highly efficient heterogeneous dual-site catalysts by leveraging the unique properties of GSH as a protective ligand by using a stepwise targeted coordination engineering approach.[217] The catalytic efficiency of the dual-site catalyst was particularly evident in the electrochemical reduction of arsenic species. Importantly, the GSH ligand played a key role in stabilizing the nanoclusters and enhancing the interaction between the catalyst and the arsenic species,[218,219] promoting bond breaking and lowering the activation energy of the reaction. This work highlights the potential of GSH as a ligand for dual-site catalysis, offering both high metal loading and stability, and sets the stage for future applications in tackling environmental contaminants like arsenic.

As nanozymes, GSH-protected MNCs mimic enzyme-like catalytic activities due to their similar hierarchical structures, where GSH can serve as the outmost structure for selective binding of substrates.[161] The precise structure and electron-donating properties of GSH enhance catalytic efficiency in reactions such as glucose oxidation[220] and H_2O_2 decomposition.[221,222]

Overall, GSH's versatile coordination chemistry makes it a bridge between biological and synthetic metal nanomaterials, enabling eco-friendly applications across disciplines. With ongoing research, GSH-protected nanomaterials are expected to address major challenges, including sustainable energy, environmental protection, and the development of high-performance functional nanomaterials.

Data availability

No primary research results, software or code have been included and no new data were generated or analyzed as part of this review.

Author contributions

J. Xie, Y. Cao, and T. Chen supervised this work. J. Xie, Z. Yang, J. Qian, and J. Lyu conceived the idea and wrote the manuscript. Q. Yao, Z. Liu, Y. Wang, Z. Yang, J. Qian, and J. Lyu participated in the literature survey. Q. Yao, Z. Liu, Y. Wang, J. Qian, and J. Lyu commented on the manuscript.

Conflicts of interest

There are no conflicts to declare.

Acknowledgements

We acknowledge the National University of Singapore and Ministry of Education, Singapore, for their financial support, through the Academic Research Fund (AcRF) Grant No. A-8000054-01-00 and No. A-8002406-00-00. We would also like to acknowledge the support from the National Natural Science Foundation of China (22071174). T. Chen acknowledges the support from the Shenzhen Science and Technology Program (JCYJ20240813113524032 and 2024SC0019) and the Chinese University of Hong Kong, Shenzhen (University Development Fund, UDF01002910). Y. Cao acknowledges the support from the National Natural Science Foundation of China (22301087).

Notes and references

1 A. Meister, On the discovery of glutathione, *Trends Biochem. Sci.*, 1988, **13**, 185–188.
2 F. G. Hopkins, On an Autoxidisable Constituent of the Cell, *Biochem. J.*, 1921, **15**, 286–305.
3 V. I. Lushchak, Glutathione homeostasis and functions: potential targets for medical interventions, *J. Amino Acids*, 2012, **2012**, 736837.
4 C. Gaucher, A. Boudier, J. Bonetti, I. Clarot, P. Leroy and M. Parent, Glutathione: Antioxidant Properties Dedicated to Nanotechnologies, *Antioxidants*, 2018, **7**, 62.
5 K. Aquilano, S. Baldelli and M. R. Ciriolo, Glutathione: new roles in redox signaling for an old antioxidant, *Front. Pharmacol*, 2014, **5**, 196.
6 H. Sies, Glutathione and its role in cellular functions, *Free Radical Biol. Med.*, 1999, **27**, 916–921.
7 L. Lin, Y. Hu, L. Zhang, Y. Huang and S. Zhao, Photoluminescence light-up detection of zinc ion and imaging in living cells based on the aggregation induced

emission enhancement of glutathione-capped copper nanoclusters, *Biosens. Bioelectron.*, 2017, **94**, 523–529.
8 J. Yang, N. Xia, X. Wang, X. Liu, A. Xu, Z. Wu and Z. Luo, One-pot one-cluster synthesis of fluorescent and biocompatible Ag_{14} nanoclusters for cancer cell imaging, *Nanoscale*, 2015, **7**, 18464–18470.
9 Y. Zheng, S. Gao and J. Y. Ying, Synthesis and Cell-Imaging Applications of Glutathione-Capped CdTe Quantum Dots, *Adv. Mater.*, 2007, **19**, 376–380.
10 C. Lennicke and H. M. Cochemé, Redox metabolism: ROS as specific molecular regulators of cell signaling and function, *Mol. Cell*, 2021, **81**, 3691–3707.
11 M. Schieber and N. S. Chandel, ROS Function in Redox Signaling and Oxidative Stress, *Curr. Biol.*, 2014, **24**, R453–R462.
12 H. Qin, V. N. Carroll, R. Sriram, J. E. Villanueva-Meyer, C. von Morze, Z. J. Wang, C. A. Mutch, K. R. Keshari, R. R. Flavell, J. Kurhanewicz and D. M. Wilson, Imaging glutathione depletion in the rat brain using ascorbate-derived hyperpolarized MR and PET probes, *Sci. Rep.*, 2018, **8**, 7928.
13 D. Aydemir, M. Hashemkhani, E. G. Durmusoglu, H. Y. Acar and N. N. Ulusu, A new substrate for glutathione reductase: Glutathione coated Ag_2S quantum dots, *Talanta*, 2019, **194**, 501–506.
14 R. Dringen, M. Brandmann, M. C. Hohnholt and E.-M. Blumrich, Glutathione-Dependent Detoxification Processes in Astrocytes, *Neurochem. Res.*, 2015, **40**, 2570–2582.
15 L. Chang, X. He, L. Chen and Y. Zhang, A novel fluorescent turn-on biosensor based on QDs@GSH–GO fluorescence resonance energy transfer for sensitive glutathione S-transferase sensing and cellular imaging, *Nanoscale*, 2017, **9**, 3881–3888.
16 D. M. Townsend, K. D. Tew and H. Tapiero, The importance of glutathione in human disease, *Biomed. Pharmacother.*, 2003, **57**, 145–155.
17 N. Ballatori, S. M. Krance, S. Notenboom, S. Shi, K. Tieu and C. L. Hammond, Glutathione dysregulation and the etiology and progression of human diseases, *Biol. Chem.*, 2009, **390**, 191–214.
18 R. Franco, O. J. Schoneveld, A. Pappa and M. I. Panayiotidis, The central role of glutathione in the pathophysiology of human diseases, *Arch. Physiol. Biochem.*, 2007, **113**, 234–258.
19 I. Rahman and W. MacNee, Regulation of redox glutathione levels and gene transcription in lung inflammation: therapeutic approaches, *Free Radical Biol. Med.*, 2000, **28**, 1405–1420.
20 D. M. Wilson, M. R. Cookson, L. Van Den Bosch, H. Zetterberg, D. M. Holtzman and I. Dewachter, Hallmarks of neurodegenerative diseases, *Cell*, 2023, **186**, 693–714.
21 I. Cacciatore, L. Baldassarre, E. Fornasari, A. Mollica and F. Pinnen, Recent Advances in the Treatment of Neurodegenerative Diseases Based on GSH Delivery Systems, *Oxid. Med. Cell. Longev.*, 2012, **1**, 240146.
22 K. Hou, J. Zhao, H. Wang, B. Li, K. Li, X. Shi, K. Wan, J. Ai, J. Lv, D. Wang, Q. Huang, H. Wang, Q. Cao, S. Liu and Z. Tang, Chiral gold nanoparticles enantioselectively rescue memory deficits in a mouse model of Alzheimer's disease, *Nat. Commun.*, 2020, **11**, 4790.
23 E. O. Olufunmilayo, M. B. Gerke-Duncan and R. M. D. Holsinger, Oxidative Stress and Antioxidants in Neurodegenerative Disorders, *Antioxidants*, 2023, **12**, 517.
24 M. Tiso, J. Tejero, S. Basu, I. Azarov, X. Wang, V. Simplaceanu, S. Frizzell, T. Jayaraman, L. Geary, C. Shapiro, C. Ho, S. Shiva, D. B. Kim-Shapiro and M. T. Gladwin, Human Neuroglobin Functions as a Redox-regulated Nitrite Reductase, *J. Biol. Chem.*, 2011, **286**, 18277–18289.
25 Y. Yu, X. Chen, Q. Yao, Y. Yu, N. Yan and J. Xie, Scalable and Precise Synthesis of Thiolated $Au_{10–12}$, Au_{15}, Au_{18}, and Au_{25} Nanoclusters via pH Controlled CO Reduction, *Chem. Mater.*, 2013, **25**, 946–952.
26 Y. Yu, Z. Luo, D. M. Chevrier, D. T. Leong, P. Zhang, D.-e. Jiang and J. Xie, Identification of a Highly Luminescent $Au_{22}(SG)_{18}$ Nanocluster, *J. Am. Chem. Soc.*, 2014, **136**, 1246–1249.
27 M. Bäumle, D. Stamou, J.-M. Segura, R. Hovius and H. Vogel, Highly Fluorescent Streptavidin-Coated CdSe Nanoparticles: Preparation in Water, Characterization, and Micropatterning, *Langmuir*, 2004, **20**, 3828–3831.
28 M. Zhao, R. Wang, B. Li, Y. Fan, Y. Wu, X. Zhu and F. Zhang, Precise In Vivo Inflammation Imaging Using In Situ Responsive Cross-linking of Glutathione-Modified Ultra-Small NIR-II Lanthanide Nanoparticles, *Angew. Chem., Int. Ed.*, 2019, **58**, 2050–2054.
29 S. Li, J. Wei, Q. Yao, X. Song, J. Xie and H. Yang, Emerging ultrasmall luminescent nanoprobes for in vivo bioimaging, *Chem. Soc. Rev.*, 2023, **52**, 1672–1696.
30 M. Baghayeri, A. Amiri, B. Maleki, Z. Alizadeh and O. Reiser, A simple approach for simultaneous detection of cadmium(II) and lead(II) based on glutathione coated magnetic nanoparticles as a highly selective electrochemical probe, *Sens. Actuators, B*, 2018, **273**, 1442–1450.
31 Z. Dai, Y. Tan, K. He, H. Chen and J. Liu, Strict DNA Valence Control in Ultrasmall Thiolate-Protected Near-Infrared-Emitting Gold Nanoparticles, *J. Am. Chem. Soc.*, 2020, **142**, 14023–14027.
32 D. M. Chevrier, L. Raich, C. Rovira, A. Das, Z. Luo, Q. Yao, A. Chatt, J. Xie, R. Jin, J. Akola and P. Zhang, Molecular-Scale Ligand Effects in Small Gold–Thiolate Nanoclusters, *J. Am. Chem. Soc.*, 2018, **140**, 15430–15436.
33 Q. Ding, W. Yang, X. Xing, H. Lin, C. Xu, L. Xu and S. Li, Modulation by Co (II) Ion of Optical Activities of L/D-glutathione (GSH)-modified Chiral Copper Nanoclusters for Sensitive Adenosine Triphosphate Detection, *Angew. Chem., Int. Ed.*, 2024, **63**, e202401032.
34 Q. Yao, M. Zhu, Z. Yang, X. Song, X. Yuan, Z. Zhang, W. Hu and J. Xie, Molecule-like synthesis of ligand-protected metal nanoclusters, *Nat. Rev. Mater.*, 2025, **10**, 89–108.

35 F. O. Silva, M. S. Carvalho, R. Mendonça, W. A. A. Macedo, K. Balzuweit, P. Reiss and M. A. Schiavon, Effect of surface ligands on the optical properties of aqueous soluble CdTe quantum dots, *Nanoscale Res. Lett.*, 2012, **7**, 536.

36 X.-C. Dai, M.-H. Huang, Y.-B. Li, T. Li, S. Hou, Z.-Q. Wei and F.-X. Xiao, Probing the Advantageous Photosensitization Effect of Metal Nanoclusters over Plasmonic Metal Nanocrystals in Photoelectrochemical Water Splitting, *J. Phys. Chem. C*, 2020, **124**, 4989–4998.

37 F. Xiao, Y. Chen, J. Qi, Q. Yao, J. Xie and X. Jiang, Multi-Targeted Peptide-Modified Gold Nanoclusters for Treating Solid Tumors in the Liver, *Adv. Mater.*, 2023, **35**, 2210412.

38 N. K. Das, S. Ghosh, A. Priya, S. Datta and S. Mukherjee, Luminescent Copper Nanoclusters as a Specific Cell-Imaging Probe and a Selective Metal Ion Sensor, *J. Phys. Chem. C*, 2015, **119**, 24657–24664.

39 X. Jiang, Q. Zhou, B. Du, S. Li, Y. Huang, Z. Chi, W. M. Lee, M. Yu and J. Zheng, Noninvasive monitoring of hepatic glutathione depletion through fluorescence imaging and blood testing, *Sci. Adv.*, 2021, **7**, eabd9847.

40 F. Yu, H. Xiang, S. He, G. Zhao, Z. Cao, L. Yang and H. Liu, Gold nanocluster-based ratiometric fluorescent probe for biosensing of Hg^{2+} ions in living organisms, *Analyst*, 2022, **147**, 2773–2778.

41 G. F. Combes, H. Fakhouri, C. Moulin, M. Girod, F. Bertorelle, S. Basu, R. Ladouce, M. P. Bakulić, Ž. S. Maršić, I. Russier-Antoine, P.-F. Brevet, P. Dugourd, A. Krisko, K. Trajković, M. Radman, V. Bonačić-Koutecký and R. Antoine, Functionalized Au_{15} nanoclusters as luminescent probes for protein carbonylation detection, *Commun. Chem.*, 2021, **4**, 69.

42 K. Yu, X. Hai, S. Yue, W. Song and S. Bi, Glutathione-activated DNA-Au nanomachine as targeted drug delivery platform for imaging-guided combinational cancer therapy, *Chem. Eng. J.*, 2021, **419**, 129535.

43 M. Hashemkhani, K. Bilici, A. Muti, A. Sennaroglu and H. Y. Acar, Ag_2S-Glutathione quantum dots for NIR image guided photothermal therapy, *New J. Chem.*, 2020, **44**, 5419–5427.

44 Y. Li, Y. Wu, J. Chen, J. Wan, C. Xiao, J. Guan, X. Song, S. Li, M. Zhang, H. Cui, T. Li, X. Yang, Z. Li and X. Yang, A Simple Glutathione-Responsive Turn-On Theranostic Nanoparticle for Dual-Modal Imaging and Chemo-Photothermal Combination Therapy, *Nano Lett.*, 2019, **19**, 5806–5817.

45 Y. Liu, Z. Yang, X. Huang, G. Yu, S. Wang, Z. Zhou, Z. Shen, W. Fan, Y. Liu, M. Davisson, H. Kalish, G. Niu, Z. Nie and X. Chen, Glutathione-Responsive Self-Assembled Magnetic Gold Nanowreath for Enhanced Tumor Imaging and Imaging-Guided Photothermal Therapy, *ACS Nano*, 2018, **12**, 8129–8137.

46 S. Jung and X. Chen, Quantum Dot-Dye Conjugates for Biosensing, Imaging, and Therapy, *Adv. Healthcare Mater.*, 2018, **7**, e1800252.

47 H. Kawasaki, S. Kumar, G. Li, C. Zeng, D. R. Kauffman, J. Yoshimoto, Y. Iwasaki and R. Jin, Generation of Singlet Oxygen by Photoexcited $Au_{25}(SR)_{18}$ Clusters, *Chem. Mater.*, 2014, **26**, 2777–2788.

48 N. Goswami, Z. Luo, X. Yuan, D. T. Leong and J. Xie, Engineering gold-based radiosensitizers for cancer radiotherapy, *Mater. Horiz.*, 2017, **4**, 817–831.

49 T.-T. Jia, G. Yang, S.-J. Mo, Z.-Y. Wang, B.-J. Li, W. Ma, Y.-X. Guo, X. Chen, X. Zhao, J.-Q. Liu and S.-Q. Zang, Atomically Precise Gold–Levonorgestrel Nanocluster as a Radiosensitizer for Enhanced Cancer Therapy, *ACS Nano*, 2019, **13**, 8320–8328.

50 X. Zhang, X. Chen, Y. W. Jiang, N. Ma, L. Y. Xia, X. Cheng, H. R. Jia, P. Liu, N. Gu, Z. Chen and F. G. Wu, Glutathione-Depleting Gold Nanoclusters for Enhanced Cancer Radiotherapy through Synergistic External and Internal Regulations, *ACS Appl. Mater. Interfaces*, 2018, **10**, 10601–10606.

51 H. Häkkinen, The gold–sulfur interface at the nanoscale, *Nat. Chem.*, 2012, **4**, 443–455.

52 J. Lee, J. Yang, S. G. Kwon and T. Hyeon, Nonclassical nucleation and growth of inorganic nanoparticles, *Nat. Rev. Mater.*, 2016, **1**, 16034.

53 J. J. Calvin, A. S. Brewer and A. P. Alivisatos, The role of organic ligand shell structures in colloidal nanocrystal synthesis, *Nat. Synth.*, 2022, **1**, 127–137.

54 M. J. Turo and J. E. Macdonald, Crystal-Bound vs Surface-Bound Thiols on Nanocrystals, *ACS Nano*, 2014, **8**, 10205–10213.

55 M. Brust, M. Walker, D. Bethell, D. J. Schiffrin and R. Whyman, Synthesis of thiol-derivatised gold nanoparticles in a two-phase Liquid–Liquid system, *J. Chem. Soc., Chem. Commun.*, 1994, 801–802.

56 S. Link, A. Beeby, S. FitzGerald, M. A. El-Sayed, T. G. Schaaff and R. L. Whetten, Visible to Infrared Luminescence from a 28-Atom Gold Cluster, *J. Phys. Chem. B*, 2002, **106**, 3410–3415.

57 B. Zhang, C. Chen, W. Chuang, S. Chen and P. Yang, Size Transformation of the $Au_{22}(SG)_{18}$ Nanocluster and Its Surface-Sensitive Kinetics, *J. Am. Chem. Soc.*, 2020, **142**, 11514–11520.

58 Y. Shichibu, Y. Negishi, H. Tsunoyama, M. Kanehara, T. Teranishi and T. Tsukuda, Extremely High Stability of Glutathionate-Protected Au_{25} Clusters Against Core Etching, *Small*, 2007, **3**, 835–839.

59 M. S. Bootharaju, V. M. Burlakov, T. M. D. Besong, C. P. Joshi, L. G. AbdulHalim, D. M. Black, R. L. Whetten, A. Goriely and O. M. Bakr, Reversible Size Control of Silver Nanoclusters via Ligand-Exchange, *Chem. Mater.*, 2015, **27**, 4289–4297.

60 K. He, Y. Tan, Z. Zhao, H. Chen and J. Liu, Weak Anchoring Sites of Thiolate-Protected Luminescent Gold Nanoparticles, *Small*, 2021, **17**, 2102481.

61 X. Le Guével, V. Trouillet, C. Spies, G. Jung and M. Schneider, Synthesis of Yellow-Emitting Platinum Nanoclusters by Ligand Etching, *J. Phys. Chem. C*, 2012, **116**, 6047–6051.

62 C. L. Torres-Martínez, L. Nguyen, R. Kho, W. Bae, K. Bozhilov, V. Klimov and R. K. Mehra, Biomolecularly capped uniformly sized nanocrystalline materials:

glutathione-capped ZnS nanocrystals, *Nanotechnology*, 1999, **10**, 340–354.

63 H. Doh, S. Hwang and S. Kim, Size-Tunable Synthesis of Nearly Monodisperse Ag_2S Nanoparticles and Size-Dependent Fate of the Crystal Structures upon Cation Exchange to $AgInS_2$ Nanoparticles, *Chem. Mater.*, 2016, **28**, 8123–8127.

64 J. Zhang, J. Li, J. Zhang, R. Xie and W. Yang, Aqueous Synthesis of ZnSe Nanocrystals by Using Glutathione As Ligand: The pH-Mediated Coordination of Zn^{2+} with Glutathione, *J. Phys. Chem. C*, 2010, **114**, 11087–11091.

65 T. G. Schaaff, G. Knight, M. N. Shafigullin, R. F. Borkman and R. L. Whetten, Isolation and Selected Properties of a 10.4 kDa Gold:Glutathione Cluster Compound, *J. Phys. Chem. B*, 1998, **102**, 10643–10646.

66 R. P. Briñas, M. Hu, L. Qian, E. S. Lymar and J. F. Hainfeld, Gold Nanoparticle Size Controlled by Polymeric Au(I) Thiolate Precursor Size, *J. Am. Chem. Soc.*, 2008, **130**, 975–982.

67 M. Yu, C. Zhou, J. Liu, J. D. Hankins and J. Zheng, Luminescent Gold Nanoparticles with pH-Dependent Membrane Adsorption, *J. Am. Chem. Soc.*, 2011, **133**, 11014–11017.

68 S. Tang, C. Peng, J. Xu, B. Du, Q. Wang, R. D. Vinluan III, M. Yu, M. J. Kim and J. Zheng, Tailoring Renal Clearance and Tumor Targeting of Ultrasmall Metal Nanoparticles with Particle Density, *Angew. Chem., Int. Ed.*, 2016, **55**, 16039–16043.

69 J.-S. Lee, H. Kim and W. R. Algar, Thiol-Ligand-Catalyzed Quenching and Etching in Mixtures of Colloidal Quantum Dots and Silver Nanoparticles, *J. Phys. Chem. C*, 2017, **121**, 28566–28575.

70 X. Yuan, M. I. Setyawati, A. S. Tan, C. N. Ong, D. T. Leong and J. Xie, Highly luminescent silver nanoclusters with tunable emissions: cyclic reduction–decomposition synthesis and antimicrobial properties, *NPG Asia Mater.*, 2013, **5**, e39.

71 D. Deng, J. Xia, J. Cao, L. Qu, J. Tian, Z. Qian, Y. Gu and Z. Gu, Forming highly fluorescent near-infrared emitting PbS quantum dots in water using glutathione as surface-modifying molecule, *J. Colloid Interface Sci.*, 2012, **367**, 234–240.

72 A. N. Jumabekov, N. Cordes, T. D. Siegler, P. Docampo, A. Ivanova, K. Fominykh, D. D. Medina, L. M. Peter and T. Bein, Passivation of PbS Quantum Dot Surface with l-Glutathione in Solid-State Quantum-Dot-Sensitized Solar Cells, *ACS Appl. Mater. Interfaces*, 2016, **8**, 4600–4607.

73 C. Zhao, Z. Bai, X. Liu, Y. Zhang, B. Zou and H. Zhong, Small GSH-Capped $CuInS_2$ Quantum Dots: MPA-Assisted Aqueous Phase Transfer and Bioimaging Applications, *ACS Appl. Mater. Interfaces*, 2015, **7**, 17623–17629.

74 H. Bao, Y. Gong, Z. Li and M. Gao, Enhancement Effect of Illumination on the Photoluminescence of Water-Soluble CdTe Nanocrystals: Toward Highly Fluorescent CdTe/CdS Core−Shell Structure, *Chem. Mater.*, 2004, **16**, 3853–3859.

75 D. R. Larson, W. R. Zipfel, R. M. Williams, S. W. Clark, M. P. Bruchez, F. W. Wise and W. W. Webb, Water-soluble quantum dots for multiphoton fluorescence imaging in vivo, *Science*, 2003, **300**, 1434–1436.

76 C. Barglik-Chory, D. Buchold, M. Schmitt, W. Kiefer, C. Heske, C. Kumpf, O. Fuchs, L. Weinhardt, A. Stahl, E. Umbach, M. Lentze, J. Geurts and G. Müller, Synthesis, structure and spectroscopic characterization of water-soluble CdS nanoparticles, *Chem. Phys. Lett.*, 2003, **379**, 443–451.

77 H. Qian, C. Dong, J. Weng and J. Ren, Facile One-Pot Synthesis of Luminescent, Water-Soluble, and Biocompatible Glutathione-Coated CdTe Nanocrystals, *Small*, 2006, **2**, 747–751.

78 Y. Zheng, Z. Yang and J. Y. Ying, Aqueous Synthesis of Glutathione-Capped ZnSe and $Zn_{1-x}Cd_xSe$ Alloyed Quantum Dots, *Adv. Mater.*, 2007, **19**, 1475–1479.

79 Y. Zheng, Z. Yang, Y. Li and J. Y. Ying, From Glutathione Capping to a Crosslinked, Phytochelatin-Like Coating of Quantum Dots, *Adv. Mater.*, 2008, **20**, 3410–3415.

80 S.-H. Choi, K. An, E.-G. Kim, J. H. Yu, J. H. Kim and T. Hyeon, Simple and Generalized Synthesis of Semiconducting Metal Sulfide Nanocrystals, *Adv. Funct. Mater.*, 2009, **19**, 1645–1649.

81 A. Delices, D. Moodelly, C. Hurot, Y. Hou, W. L. Ling, C. Saint-Pierre, D. Gasparutto, G. Nogues, P. Reiss and K. Kheng, Aqueous Synthesis of DNA-Functionalized Near-Infrared $AgInS_2$/ZnS Core/Shell Quantum Dots, *ACS Appl. Mater. Interfaces*, 2020, **12**, 44026–44038.

82 M. Wang, L. Nian, Y. Cheng, B. Yuan, S. Cheng and C. Cao, Encapsulation of colloidal semiconductor quantum dots into metal-organic frameworks for enhanced antibacterial activity through interfacial electron transfer, *Chem. Eng. J.*, 2021, **426**, 130832.

83 X. Luo and J. Liu, Ultrasmall Luminescent Metal Nanoparticles: Surface Engineering Strategies for Biological Targeting and Imaging, *Adv. Sci.*, 2022, **9**, 2103971.

84 J. Liu, P. N. Duchesne, M. Yu, X. Jiang, X. Ning, R. D. Vinluan Iii, P. Zhang and J. Zheng, Luminescent Gold Nanoparticles with Size-Independent Emission, *Angew. Chem., Int. Ed.*, 2016, **55**, 8894–8898.

85 R. Jin, H. Qian, Z. Wu, Y. Zhu, M. Zhu, A. Mohanty and N. Garg, Size Focusing: A Methodology for Synthesizing Atomically Precise Gold Nanoclusters, *J. Phys. Chem. Lett.*, 2010, **1**, 2903–2910.

86 T. G. Schaaff and R. L. Whetten, Giant Gold−Glutathione Cluster Compounds: Intense Optical Activity in Metal-Based Transitions, *J. Phys. Chem. B*, 2000, **104**, 2630–2641.

87 Y. Negishi, K. Nobusada and T. Tsukuda, Glutathione-Protected Gold Clusters Revisited: Bridging the Gap between Gold(I)−Thiolate Complexes and Thiolate-Protected Gold Nanocrystals, *J. Am. Chem. Soc.*, 2005, **127**, 5261–5270.

88 S. Kumar, M. D. Bolan and T. P. Bigioni, Glutathione-Stabilized Magic-Number Silver Cluster Compounds, *J. Am. Chem. Soc.*, 2010, **132**, 13141–13143.

89 T. Chen, Z. Luo, Q. Yao, A. X. H. Yeo and J. Xie, Synthesis of thiolate-protected Au nanoparticles revisited: U-shape

trend between the size of nanoparticles and thiol-to-Au ratio, *Chem. Commun.*, 2016, **52**, 9522–9525.

90 T. Chen, V. Fung, Q. Yao, Z. Luo, D.-e. Jiang and J. Xie, Synthesis of Water-Soluble $[Au_{25}(SR)_{18}]^-$ Using a Stoichiometric Amount of $NaBH_4$, *J. Am. Chem. Soc.*, 2018, **140**, 11370–11377.

91 K. Jin, W. Wang, G. Qi, X. Peng, H. Gao, H. Zhu, X. He, H. Zou, L. Yang, J. Yuan, L. Zhang, H. Chen and X. Qu, An explainable machine-learning approach for revealing the complex synthesis path–property relationships of nanomaterials, *Nanoscale*, 2023, **15**, 15358–15367.

92 Q. Yao, Y. Yu, X. Yuan, Y. Yu, J. Xie and J. Y. Lee, Two-Phase Synthesis of Small Thiolate-Protected Au_{15} and Au_{18} Nanoclusters, *Small*, 2013, **9**, 2696–2701.

93 C. Zhou, C. Sun, M. Yu, Y. Qin, J. Wang, M. Kim and J. Zheng, Luminescent Gold Nanoparticles with Mixed Valence States Generated from Dissociation of Polymeric Au(I) Thiolates, *J. Phys. Chem. C*, 2010, **114**, 7727–7732.

94 Z. Wu, Q. Yao, O. J. H. Chai, N. Ding, W. Xu, S. Zang and J. Xie, Unraveling the Impact of Gold(I)–Thiolate Motifs on the Aggregation-Induced Emission of Gold Nanoclusters, *Angew. Chem., Int. Ed.*, 2020, **59**, 9934–9939.

95 Z. Luo, X. Yuan, Y. Yu, Q. Zhang, D. T. Leong, J. Y. Lee and J. Xie, From Aggregation-Induced Emission of Au(I)–Thiolate Complexes to Ultrabright Au(0)@Au(I)–Thiolate Core–Shell Nanoclusters, *J. Am. Chem. Soc.*, 2012, **134**, 16662–16670.

96 K. Edinger, A. Goelzhaeuser, K. Demota, C. Woell and M. Grunze, Formation of self-assembled monolayers of n-alkanethiols on gold: a scanning tunneling microscopy study on the modification of substrate morphology, *Langmuir*, 1993, **9**, 4–8.

97 T. G. Schaaff and R. L. Whetten, Controlled Etching of Au:SR Cluster Compounds, *J. Phys. Chem. B*, 1999, **103**, 9394–9396.

98 Y. Cao, T. Liu, T. Chen, B. Zhang, D.-e. Jiang and J. Xie, Revealing the etching process of water-soluble Au_{25} nanoclusters at the molecular level, *Nat. Commun.*, 2021, **12**, 3212.

99 T. A. Dreier and C. J. Ackerson, Radicals Are Required for Thiol Etching of Gold Particles, *Angew. Chem., Int. Ed.*, 2015, **54**, 9249–9252.

100 E. S. Shibu, M. A. H. Muhammed, T. Tsukuda and T. Pradeep, Ligand Exchange of $Au_{25}SG_{18}$ Leading to Functionalized Gold Clusters: Spectroscopy, Kinetics, and Luminescence, *J. Phys. Chem. C*, 2008, **112**, 12168–12176.

101 M. A. Habeeb Muhammed, S. Ramesh, S. S. Sinha, S. K. Pal and T. Pradeep, Two distinct fluorescent quantum clusters of gold starting from metallic nanoparticles by pH-dependent ligand etching, *Nano Res.*, 2008, **1**, 333–340.

102 X. Le Guével, B. Hötzer, G. Jung, K. Hollemeyer, V. Trouillet and M. Schneider, Formation of Fluorescent Metal (Au, Ag) Nanoclusters Capped in Bovine Serum Albumin Followed by Fluorescence and Spectroscopy, *J. Phys. Chem. C*, 2011, **115**, 10955–10963.

103 X. Le Guével, C. Spies, N. Daum, G. Jung and M. Schneider, Highly fluorescent silver nanoclusters stabilized by glutathione: a promising fluorescent label for bioimaging, *Nano Res.*, 2012, **5**, 379–387.

104 X. Yuan, B. Zhang, Z. Luo, Q. Yao, D. T. Leong, N. Yan and J. Xie, Balancing the Rate of Cluster Growth and Etching for Gram-Scale Synthesis of Thiolate-Protected Au_{25} Nanoclusters with Atomic Precision, *Angew. Chem., Int. Ed.*, 2014, **53**, 4623–4627.

105 S. K. Katla, J. Zhang, E. Castro, R. A. Bernal and X. Li, Atomically Precise $Au_{25}(SG)_{18}$ Nanoclusters: Rapid Single-Step Synthesis and Application in Photothermal Therapy, *ACS Appl. Mater. Interfaces*, 2018, **10**, 75–82.

106 S. R. Bhattacharya, K. Bhattacharya, V. J. Xavier, A. Ziarati, D. Picard and T. Bürgi, The Atomically Precise Gold/Captopril Nanocluster $Au_{25}(Capt)_{18}$ Gains Anticancer Activity by Inhibiting Mitochondrial Oxidative Phosphorylation, *ACS Appl. Mater. Interfaces*, 2022, **14**, 29521–29536.

107 Y. Shichibu, Y. Negishi, T. Tsukuda and T. Teranishi, Large-Scale Synthesis of Thiolated Au_{25} Clusters via Ligand Exchange Reactions of Phosphine-Stabilized Au_{11} Clusters, *J. Am. Chem. Soc.*, 2005, **127**, 13464–13465.

108 L. C. McKenzie, T. O. Zaikova and J. E. Hutchison, Structurally similar triphenylphosphine-stabilized undecagolds, $Au_{11}(PPh_3)_7Cl_3$ and $[Au_{11}(PPh_3)_8Cl_2]Cl$, exhibit distinct ligand exchange pathways with glutathione, *J. Am. Chem. Soc.*, 2014, **136**, 13426–13435.

109 H. Qian, M. Zhu, U. N. Andersen and R. Jin, Facile, Large-Scale Synthesis of Dodecanethiol-Stabilized Au38 Clusters, *J. Phys. Chem. A*, 2009, **113**, 4281–4284.

110 S. Chen, S. Wang, J. Zhong, Y. Song, J. Zhang, H. Sheng, Y. Pei and M. Zhu, The Structure and Optical Properties of the $[Au_{18}(SR)_{14}]$ Nanocluster, *Angew. Chem., Int. Ed.*, 2015, **54**, 3145–3149.

111 S. Yang, S. Chen, L. Xiong, C. Liu, H. Yu, S. Wang, N. L. Rosi, Y. Pei and M. Zhu, Total Structure Determination of $Au_{16}(S\text{-}Adm)_{12}$ and $Cd_1Au_{14}(StBu)_{12}$ and Implications for the Structure of $Au_{15}(SR)_{13}$, *J. Am. Chem. Soc.*, 2018, **140**, 10988–10994.

112 V. Truttmann, S. Pollitt, H. Drexler, S. P. Nandan, D. Eder, N. Barrabés and G. Rupprechter, Selective ligand exchange synthesis of $Au_{16}(2\text{-}PET)_{14}$ from $Au_{15}(SG)_{13}$, *J. Chem. Phys.*, 2021, **155**, 161102.

113 V. Rojas-Cervellera, L. Raich, J. Akola and C. Rovira, The molecular mechanism of the ligand exchange reaction of an antibody against a glutathione-coated gold cluster, *Nanoscale*, 2017, **9**, 3121–3127.

114 Y. Wang and T. Bürgi, Ligand exchange reactions on thiolate-protected gold nanoclusters, *Nanoscale Adv.*, 2021, **3**, 2710–2727.

115 Y.-F. Liu and J.-S. Yu, In situ synthesis of highly luminescent glutathione-capped CdTe/ZnS quantum dots with biocompatibility, *J. Colloid Interface Sci.*, 2010, **351**, 1–9.

116 N.-N. Zhang, H.-R. Sun, S. Liu, Y.-C. Xing, J. Lu, F. Peng, C.-L. Han, Z. Wei, T. Sun, B. Yang and K. Liu, Gold Nanoparticle Enantiomers and Their Chiral-Morphology

Dependence of Cellular Uptake, *CCS Chem.*, 2022, **4**, 660–670.
117 Y. Zheng, Q. Wang, Y. Sun, J. Huang, J. Ji, Z.-J. Wang, Y. Wang and H. Chen, Chiral Active Surface Growth via Glutathione Control, *Adv. Opt. Mater.*, 2023, **11**, 2202858.
118 H. Tang, Q. Li, W. Yan and X. Jiang, Reversing the Chirality of Surface Ligands Can Improve the Biosafety and Pharmacokinetics of Cationic Gold Nanoclusters, *Angew. Chem., Int. Ed.*, 2021, **60**, 13829–13834.
119 Z. Wang, Y. Tian, J. Hao, Y. Liu, J. Tang, Z. Xu, Y. Liu, B. Tang, X. Huang, N. Zhu, Z. Li, L. Hu, L. Li, Y. Wang and G. Jiang, Chiral Nanoclusters as Alternative Therapeutic Strategies to Confront the Health Threat from Antibiotic-Resistant Pathogens, *ACS Nano*, 2024, **18**, 7253–7266.
120 A. Samanta, Z. Deng and Y. Liu, Infrared emitting quantum dots: DNA conjugation and DNA origami directed self-assembly, *Nanoscale*, 2014, **6**, 4486–4490.
121 Y.-F. Liu and J.-S. Yu, Selective synthesis of CdTe and high luminescence CdTe/CdS quantum dots: The effect of ligands, *J. Colloid Interface Sci.*, 2009, **333**, 690–698.
122 Y. Wang, X. Liang, X. Ma, Y. Hu, X. Hu, X. Li and J. Fan, Simple and greener synthesis of highly photoluminescence Mn^{2+}-doped ZnS quantum dots and its surface passivation mechanism, *Appl. Surf. Sci.*, 2014, **316**, 54–61.
123 Y. Chen, L. Huang, S. Li and D. Pan, Aqueous synthesis of glutathione-capped Cu^{+} and Ag^{+}-doped $Zn_xCd_{1-x}S$ quantum dots with full color emission, *J. Mater. Chem. C*, 2013, **1**, 751–756.
124 W. Li, J. Liu, K. Sun, H. Dou and K. Tao, Highly fluorescent water soluble $Cd_xZn_{1-x}Te$ alloyed quantum dots prepared in aqueous solution: one-step synthesis and the alloy effect of Zn, *J. Mater. Chem.*, 2010, **20**, 2133–2138.
125 N. Tsolekile, S. Parani, N. Vuyelwa, R. Maluleke, M. Matoetoe, S. Songca and O. S. Oluwafemi, Synthesis, structural and fluorescence optimization of ternary Cu–In–S quantum dots passivated with ZnS, *J. Lumin.*, 2020, **227**, 117541.
126 D. Su, L. Wang, M. Li, S. Mei, X. Wei, H. Dai, Z. Hu, F. Xie and R. Guo, Highly luminescent water-soluble $AgInS_2$/ZnS quantum dots-hydrogel composites for warm white LEDs, *J. Alloys Compd.*, 2020, **824**, 153896.
127 O. Stroyuk, A. Raevskaya, F. Spranger, O. Selyshchev, V. Dzhagan, S. Schulze, D. R. T. Zahn and A. Eychmüller, Origin and Dynamics of Highly Efficient Broadband Photoluminescence of Aqueous Glutathione-Capped Size-Selected Ag–In–S Quantum Dots, *J. Phys. Chem. C*, 2018, **122**, 13648–13658.
128 Y. G. Srinivasulu, N. Goswami, Q. Yao and J. Xie, High-Yield Synthesis of AIE-Type $Au_{22}(SG)_{18}$ Nanoclusters through Precursor Engineering and Its pH-Dependent Size Transformation, *J. Phys. Chem. C*, 2021, **125**, 4066–4076.
129 K. Pyo, V. D. Thanthirige, K. Kwak, P. Pandurangan, G. Ramakrishna and D. Lee, Ultrabright Luminescence from Gold Nanoclusters: Rigidifying the Au(I)–Thiolate Shell, *J. Am. Chem. Soc.*, 2015, **137**, 8244–8250.
130 H. Deng, K. Huang, L. Xiu, W. Sun, Q. Yao, X. Fang, X. Huang, H. A. A. Noreldeen, H. Peng, J. Xie and W. Chen, Bis-Schiff base linkage-triggered highly bright luminescence of gold nanoclusters in aqueous solution at the single-cluster level, *Nat. Commun.*, 2022, **13**, 3381.
131 M. Zhou and Y. Song, Origins of Visible and Near-Infrared Emissions in $[Au_{25}(SR)_{18}]^{-}$ Nanoclusters, *J. Phys. Chem. Lett.*, 2021, **12**, 1514–1519.
132 W. Chen, X. Tu and X. Guo, Fluorescent gold nanoparticles-based fluorescence sensor for Cu^{2+} ions, *Chem. Commun.*, 2009, **13**, 1736–1738.
133 T. Luo, S. Zhang, Y. Wang, M. Wang, M. Liao and X. Kou, Glutathione-stabilized Cu nanocluster-based fluorescent probe for sensitive and selective detection of Hg^{2+} in water, *Luminescence*, 2017, **32**, 1092–1099.
134 R. Rossetti, S. Nakahara and L. E. Brus, Quantum size effects in the redox potentials, resonance Raman spectra, and electronic spectra of CdS crystallites in aqueous solution, *J. Chem. Phys.*, 1983, **79**, 1086–1088.
135 J. M. Pietryga, Y.-S. Park, J. Lim, A. F. Fidler, W. K. Bae, S. Brovelli and V. I. Klimov, Spectroscopic and Device Aspects of Nanocrystal Quantum Dots, *Chem. Rev.*, 2016, **116**, 10513–10622.
136 R. Freeman and I. Willner, Optical molecular sensing with semiconductor quantum dots (QDs), *Chem. Soc. Rev.*, 2012, **41**, 4067–4085.
137 D. A. Hines and P. V. Kamat, Recent Advances in Quantum Dot Surface Chemistry, *ACS Appl. Mater. Interfaces*, 2014, **6**, 3041–3057.
138 A. Samanta, Z. Deng and Y. Liu, Aqueous Synthesis of Glutathione-Capped CdTe/CdS/ZnS and CdTe/CdSe/ZnS Core/Shell/Shell Nanocrystal Heterostructures, *Langmuir*, 2012, **28**, 8205–8215.
139 L. Dhamo, F. Carulli, P. Nickl, K. D. Wegner, V.-D. Hodoroaba, C. Würth, S. Brovelli and U. Resch-Genger, Efficient Luminescent Solar Concentrators Based on Environmentally Friendly Cd-Free Ternary AIS/ZnS Quantum Dots, *Adv. Opt. Mater.*, 2021, **9**, 2100587.
140 L.-L. Li, Y.-H. Cui, J.-J. Chen and H.-Q. Yu, Roles of glutathione and L-cysteine in the biomimetic green synthesis of CdSe quantum dots, *Front. Environ. Sci. Eng.*, 2017, **11**, 7.
141 O. Raievska, O. Stroyuk, Y. Azhniuk, D. Solonenko, A. Barabash, C. J. Brabec and D. R. T. Zahn, Composition-Dependent Optical Band Bowing, Vibrational, and Photochemical Behavior of Aqueous Glutathione-Capped (Cu, Ag)–In–S Quantum Dots, *J. Phys. Chem. C*, 2020, **124**, 19375–19388.
142 R. R. Nasaruddin, T. Chen, N. Yan and J. Xie, Roles of thiolate ligands in the synthesis, properties and catalytic application of gold nanoclusters, *Coord. Chem. Rev.*, 2018, **368**, 60–79.
143 T. Chen, H. Lin, Y. Cao, Q. Yao and J. Xie, Interactions of Metal Nanoclusters with Light: Fundamentals and Applications, *Adv. Mater.*, 2022, **34**, 2103918.
144 Z. Wu and R. Jin, On the Ligand's Role in the Fluorescence of Gold Nanoclusters, *Nano Lett.*, 2010, **10**, 2568–2573.

145 J. X. Dong, Z. F. Gao, Y. Zhang, B. L. Li, W. Zhang, J. L. Lei, N. B. Li and H. Q. Luo, The pH-switchable agglomeration and dispersion behavior of fluorescent Ag nanoclusters and its applications in urea and glucose biosensing, *NPG Asia Mater.*, 2016, **8**, e335.

146 D. Ding, K. Li, B. Liu and B. Z. Tang, Bioprobes Based on AIE Fluorogens, *Acc. Chem. Res.*, 2013, **46**, 2441–2453.

147 J. Luo, Z. Xie, J. W. Y. Lam, L. Cheng, H. Chen, C. Qiu, H. S. Kwok, X. Zhan, Y. Liu, D. Zhu and B. Z. Tang, Aggregation-induced emission of 1-methyl-1,2,3,4,5-pentaphenylsilole, *Chem. Commun.*, 2001, 1740–1741.

148 O. Raize, Y. Argaman and S. Yannai, Mechanisms of biosorption of different heavy metals by brown marine macroalgae, *Biotechnol. Bioeng.*, 2004, **87**, 451–458.

149 W. Zhang, Y. Shi, J. Zhang, G. Shi, X. Qiao, Y. He, J. W. Y. Lam, Z. Zhao, J. Xie, X. Pang and B. Z. Tang, Precision Synthesis of Ultrastable Hydrophilic Metal Nanocluster Assemblies, *Macromolecules*, 2024, **57**, 4556–4566.

150 N. Goswami, Q. Yao, Z. Luo, J. Li, T. Chen and J. Xie, Luminescent Metal Nanoclusters with Aggregation-Induced Emission, *J. Phys. Chem. Lett.*, 2016, **7**, 962–975.

151 M. Wu, J. Zhao, D. M. Chevrier, P. Zhang and L. Liu, Luminescent Au(I)–Thiolate Complexes through Aggregation-Induced Emission: The Effect of pH during and Post Synthesis, *J. Phys. Chem. C*, 2019, **123**, 6010–6017.

152 X.-S. Han, X. Luan, H.-F. Su, J.-J. Li, S.-F. Yuan, Z. Lei, Y. Pei and Q.-M. Wang, Structure Determination of Alkynyl-Protected Gold Nanocluster $Au_{22}(tBuC{\equiv}C)_{18}$ and Its Thermochromic Luminescence, *Angew. Chem., Int. Ed.*, 2020, **59**, 2309–2312.

153 N.-N. Zhang, H.-R. Sun, Y. Xue, F. Peng and K. Liu, Tuning the Chiral Morphology of Gold Nanoparticles with Oligomeric Gold–Glutathione Complexes, *J. Phys. Chem. C*, 2021, **125**, 10708–10715.

154 J. Zheng, C. Boukouvala, G. R. Lewis, Y. Ma, Y. Chen, E. Ringe, L. Shao, Z. Huang and J. Wang, Halide-assisted differential growth of chiral nanoparticles with threefold rotational symmetry, *Nat. Commun.*, 2023, **14**, 3783.

155 Y. L. Engel, D. Feferman, M. Ghalawat, E. Y. Santiago, O. Avalos-Ovando, A. O. Govorov and G. Markovich, Reshaping and induction of optical activity in gold@silver nanocuboids by chiral glutathione molecules, *J. Chem. Phys.*, 2024, **160**, 024706.

156 M. Monti, M. F. Matus, S. Malola, A. Fortunelli, M. Aschi, M. Stener and H. Häkkinen, What Contributes to the Measured Chiral Optical Response of the Glutathione-Protected Au_{25} Nanocluster?, *ACS Nano*, 2023, **17**, 11481–11491.

157 X. Zhu, Z. Zhao, X. Chi and J. Gao, Facile, sensitive, and ratiometric detection of mercuric ions using GSH-capped semiconductor quantum dots, *Analyst*, 2013, **138**, 3230–3237.

158 E. Mohamed Ali, Y. Zheng, H.-h. Yu and J. Y. Ying, Ultrasensitive Pb^{2+} Detection by Glutathione-Capped Quantum Dots, *Anal. Chem.*, 2007, **79**, 9452–9458.

159 K. Pyo, H. Xu, S. M. Han, S. Saxena, S. Y. Yoon, G. Wiederrecht, G. Ramakrishna and D. Lee, Synthesis and Photophysical Properties of Light-Harvesting Gold Nanoclusters Fully Functionalized with Antenna Chromophores, *Small*, 2021, **17**, 2004836.

160 M. Wang, B. Duan, Y. Li, S. Jiang, Z. Huang and W. Yang, Glutathione-Capped Au Nanoclusters Embedded in NaCl Crystals for White Light-Emitting Devices, *ACS Appl. Nano Mater.*, 2021, **4**, 7486–7492.

161 X. Pan, Y. Yao, M. Zhang, X. Yuan, Q. Yao and W. Hu, Enzyme-mimic catalytic activities and biomedical applications of noble metal nanoclusters, *Nanoscale*, 2024, **16**, 8196–8215.

162 Y. Shi, Z. Wu, M. Qi, C. Liu, W. Dong, W. Sun, X. Wang, F. Jiang, Y. Zhong, D. Nan, Y. Zhang, C. Li, L. Wang and X. Bai, Multiscale Bioresponses of Metal Nanoclusters, *Adv. Mater.*, 2024, **36**, 2310529.

163 G. Yang, Z. Wang, F. Du, F. Jiang, X. Yuan and J. Y. Ying, Ultrasmall Coinage Metal Nanoclusters as Promising Theranostic Probes for Biomedical Applications, *J. Am. Chem. Soc.*, 2023, **145**, 11879–11898.

164 W. Wang, W. Yu, G. Li, H. Huang, X. Song, L. Yu and Y. Chen, Engineering versatile nano-bacteria hybrids for efficient tumor therapy, *Coord. Chem. Rev.*, 2023, **488**, 215178.

165 B. Du, M. Yu and J. Zheng, Transport and interactions of nanoparticles in the kidneys, *Nat. Rev. Mater.*, 2018, **3**, 358–374.

166 A.-H. Lu, E. L. Salabas and F. Schüth, Magnetic Nanoparticles: Synthesis, Protection, Functionalization, and Application, *Angew. Chem., Int. Ed.*, 2007, **46**, 1222–1244.

167 Y. Liu, L. Wang, Q. Ma, X. Xu, X. Gao, H. Zhu, T. Feng, X. Dou, M. Eguchi, Y. Yamauchi and X. Yuan, Simultaneous generation of residue-free reactive oxygen species and bacteria capture for efficient electrochemical water disinfection, *Nat. Commun.*, 2024, **15**, 10175.

168 S. Wang, F. Zhang, G. Yu, Z. Wang, O. Jacobson, Y. Ma, R. Tian, H. Deng, W. Yang, Z.-Y. Chen and X. Chen, Zwitterionic-to-cationic charge conversion polyprodrug nanomedicine for enhanced drug delivery, *Theranostics*, 2020, **10**, 6629–6637.

169 J. Liu, M. Yu, C. Zhou, S. Yang, X. Ning and J. Zheng, Passive Tumor Targeting of Renal-Clearable Luminescent Gold Nanoparticles: Long Tumor Retention and Fast Normal Tissue Clearance, *J. Am. Chem. Soc.*, 2013, **135**, 4978–4981.

170 C. Zhou, M. Long, Y. Qin, X. Sun and J. Zheng, Luminescent Gold Nanoparticles with Efficient Renal Clearance, *Angew. Chem., Int. Ed.*, 2011, **50**, 3168–3172.

171 M. Yu, J. Xu and J. Zheng, Renal Clearable Luminescent Gold Nanoparticles: From the Bench to the Clinic, *Angew. Chem., Int. Ed.*, 2019, **58**, 4112–4128.

172 A. Zhang, K. Meng, Y. Liu, Y. Pan, W. Qu, D. Chen and S. Xie, Absorption, distribution, metabolism, and excretion of nanocarriers in vivo and their influences, *Adv. Colloid Interface Sci.*, 2020, **284**, 102261.

173 X. Huang, I. H. El-Sayed, W. Qian and M. A. El-Sayed, Cancer Cell Imaging and Photothermal Therapy in the Near-Infrared Region by Using Gold Nanorods, *J. Am. Chem. Soc.*, 2006, **128**, 2115–2120.

174 H. Zhang, H. Liu, Z. Tian, D. Lu, Y. Yu, S. Cestellos-Blanco, K. K. Sakimoto and P. Yang, Bacteria photosensitized by intracellular gold nanoclusters for solar fuel production, *Nat. Nanotechnol.*, 2018, **13**, 900–905.

175 M. Yu, J. Liu, X. Ning and J. Zheng, High-contrast Noninvasive Imaging of Kidney Clearance Kinetics Enabled by Renal Clearable Nanofluorophores, *Angew. Chem., Int. Ed.*, 2015, **54**, 15434–15438.

176 Z. Fang, C. Wang, J. Yang, Z. Song, C. Xie, Y. Ji, Z. Wang, X. Du, Q. Zheng, C. Chen, Z. Hu and Y. Zhong, Oxyhaemoglobin saturation NIR-II imaging for assessing cancer metabolism and predicting the response to immunotherapy, *Nat. Nanotechnol.*, 2024, **19**, 124–130.

177 R. Cai, J. Ren, M. Guo, T. Wei, Y. Liu, C. Xie, P. Zhang, Z. Guo, A. J. Chetwynd, P. C. Ke, I. Lynch and C. Chen, Dynamic intracellular exchange of nanomaterials' protein corona perturbs proteostasis and remodels cell metabolism, *Proc. Natl. Acad. Sci. U. S. A.*, 2022, **119**, e2200363119.

178 M. Emanuele and B. Balasubramaniam, Differential Effects of Commercial-Grade and Purified Poloxamer 188 on Renal Function, *Drugs R&D*, 2014, **14**, 73–83.

179 B. Du, X. Jiang, A. Das, Q. Zhou, M. Yu, R. Jin and J. Zheng, Glomerular barrier behaves as an atomically precise bandpass filter in a sub-nanometre regime, *Nat. Nanotechnol.*, 2017, **12**, 1096–1102.

180 Y. Matsumura and H. Maeda, A new concept for macromolecular therapeutics in cancer chemotherapy: mechanism of tumoritropic accumulation of proteins and the antitumor agent smancs, *Cancer Res.*, 1986, **46**, 6387–6392.

181 L. E. Gerlowski and R. K. Jain, Microvascular permeability of normal and neoplastic tissues, *Microvasc. Res.*, 1986, **31**, 288–305.

182 H. Maeda, Toward a full understanding of the EPR effect in primary and metastatic tumors as well as issues related to its heterogeneity, *Adv. Drug Delivery Rev.*, 2015, **91**, 3–6.

183 N. Bertrand, J. Wu, X. Xu, N. Kamaly and O. C. Farokhzad, Cancer nanotechnology: The impact of passive and active targeting in the era of modern cancer biology, *Adv. Drug Delivery Rev.*, 2014, **66**, 2–25.

184 J. Shi, P. W. Kantoff, R. Wooster and O. C. Farokhzad, Cancer nanomedicine: progress, challenges and opportunities, *Nat. Rev. Cancer*, 2017, **17**, 20–37.

185 H. Soo Choi, W. Liu, P. Misra, E. Tanaka, J. P. Zimmer, B. Itty Ipe, M. G. Bawendi and J. V. Frangioni, Renal clearance of quantum dots, *Nat. Biotechnol.*, 2007, **25**, 1165–1170.

186 R. D. Vinluan III, J. Liu, C. Zhou, M. Yu, S. Yang, A. Kumar, S. Sun, A. Dean, X. Sun and J. Zheng, Glutathione-Coated Luminescent Gold Nanoparticles: A Surface Ligand for Minimizing Serum Protein Adsorption, *ACS Appl. Mater. Interfaces*, 2014, **6**, 11829–11833.

187 X. Cheng, H.-D. Xu, H.-H. Ran, G. Liang and F.-G. Wu, Glutathione-Depleting Nanomedicines for Synergistic Cancer Therapy, *ACS Nano*, 2021, **15**, 8039–8068.

188 A. Baghdasaryan, F. Wang, F. Ren, Z. Ma, J. Li, X. Zhou, L. Grigoryan, C. Xu and H. Dai, Phosphorylcholine-conjugated gold-molecular clusters improve signal for Lymph Node NIR-II fluorescence imaging in preclinical cancer models, *Nat. Commun.*, 2022, **13**, 5613.

189 Y. Li, Y. Zhou, H.-Y. Wang, S. Perrett, Y. Zhao, Z. Tang and G. Nie, Chirality of Glutathione Surface Coating Affects the Cytotoxicity of Quantum Dots, *Angew. Chem., Int. Ed.*, 2011, **50**, 5860–5864.

190 L. Yuan, F. Zhang, X. Qi, Y. Yang, C. Yan, J. Jiang and J. Deng, Chiral polymer modified nanoparticles selectively induce autophagy of cancer cells for tumor ablation, *J. Nanobiotechnol.*, 2018, **16**, 55.

191 L. Xu, H. Gao, W. Zhan, Y. Deng, X. Liu, Q. Jiang, X. Sun, J.-J. Xu and G. Liang, Dual Aggregations of a Near-Infrared Aggregation-Induced Emission Luminogen for Enhanced Imaging of Alzheimer's Disease, *J. Am. Chem. Soc.*, 2023, **145**, 27748–27756.

192 L. Qin, X. He, L. Chen and Y. Zhang, Turn-on Fluorescent Sensing of Glutathione S-Transferase at near-Infrared Region Based on FRET between Gold Nanoclusters and Gold Nanorods, *ACS Appl. Mater. Interfaces*, 2015, **7**, 5965–5971.

193 D. Li, Q. Liu, Q. Qi, H. Shi, E.-C. Hsu, W. Chen, W. Yuan, Y. Wu, S. Lin, Y. Zeng, Z. Xiao, L. Xu, Y. Zhang, T. Stoyanova, W. Jia and Z. Cheng, Gold Nanoclusters for NIR-II Fluorescence Imaging of Bones, *Small*, 2020, **16**, 2003851.

194 C. Zhou, G. Hao, P. Thomas, J. Liu, M. Yu, S. Sun, O. K. Öz, X. Sun and J. Zheng, Near-Infrared Emitting Radioactive Gold Nanoparticles with Molecular Pharmacokinetics, *Angew. Chem., Int. Ed.*, 2012, **51**, 10118–10122.

195 H. Liu, G. Hong, Z. Luo, J. Chen, J. Chang, M. Gong, H. He, J. Yang, X. Yuan, L. Li, X. Mu, J. Wang, W. Mi, J. Luo, J. Xie and X.-D. Zhang, Atomic-Precision Gold Clusters for NIR-II Imaging, *Adv. Mater.*, 2019, **31**, 1901015.

196 X. Jiang, B. Du, S. Tang, J.-T. Hsieh and J. Zheng, Photoacoustic Imaging of Nanoparticle Transport in the Kidneys at High Temporal Resolution, *Angew. Chem., Int. Ed.*, 2019, **58**, 5994–6000.

197 X. Jiang, B. Du and J. Zheng, Glutathione-mediated biotransformation in the liver modulates nanoparticle transport, *Nat. Nanotechnol.*, 2019, **14**, 874–882.

198 A. A. Sousa, J. T. Morgan, P. H. Brown, A. Adams, M. P. S. Jayasekara, G. Zhang, C. J. Ackerson, M. J. Kruhlak and R. D. Leapman, Synthesis, Characterization, and Direct Intracellular Imaging of Ultrasmall and Uniform Glutathione-Coated Gold Nanoparticles, *Small*, 2012, **8**, 2277–2286.

199 Y. G. Srinivasulu, A. Mozhi, N. Goswami, Q. Yao and J. Xie, Traceable Nanocluster–Prodrug Conjugate for Chemo-photodynamic Combinatorial Therapy of Non-small Cell Lung Cancer, *ACS Appl. Bio Mater.*, 2021, **4**, 3232–3245.

200 X. Jiang, B. Du, Y. Huang, M. Yu and J. Zheng, Cancer Photothermal Therapy with ICG-Conjugated Gold Nanoclusters, *Bioconjugate Chem.*, 2020, **31**, 1522–1528.
201 Y. Yang, S. Wang, S. Chen, Y. Shen and M. Zhu, Switching the subcellular organelle targeting of atomically precise gold nanoclusters by modifying the capping ligand, *Chem. Commun.*, 2018, **54**, 9222–9225.
202 Z. Qin, T. Du, Y. Zheng, P. Luo, J. Zhang, M. Xie, Y. Zhang, Y. Du, L. Yin, D. Cui, Q. Lu, M. Lu, X. Wang and H. Jiang, Glutathione Induced Transformation of Partially Hollow Gold–Silver Nanocages for Cancer Diagnosis and Photothermal Therapy, *Small*, 2019, **15**, 1902755.
203 I. A. Mir, V. S. Radhakrishanan, K. Rawat, T. Prasad and H. B. Bohidar, Bandgap Tunable AgInS based Quantum Dots for High Contrast Cell Imaging with Enhanced Photodynamic and Antifungal Applications, *Sci. Rep.*, 2018, **8**, 9322.
204 X.-D. Zhang, J. Chen, Z. Luo, D. Wu, X. Shen, S.-S. Song, Y.-M. Sun, P.-X. Liu, J. Zhao, S. Huo, S. Fan, F. Fan, X.-J. Liang and J. Xie, Enhanced Tumor Accumulation of Sub-2 nm Gold Nanoclusters for Cancer Radiation Therapy, *Adv. Healthcare Mater.*, 2014, **3**, 133–141.
205 X.-D. Zhang, Z. Luo, J. Chen, X. Shen, S. Song, Y. Sun, S. Fan, F. Fan, D. T. Leong and J. Xie, Ultrasmall $Au_{10-12}(SG)_{10-12}$ Nanomolecules for High Tumor Specificity and Cancer Radiotherapy, *Adv. Mater.*, 2014, **26**, 4565–4568.
206 Z. Yang, A. Shi, R. Zhang, Z. Ji, J. Li, J. Lyu, J. Qian, T. Chen, X. Wang, F. You and J. Xie, When Metal Nanoclusters Meet Smart Synthesis, *ACS Nano*, 2024, **18**, 27138–27166.
207 E. M. Williamson, Z. Sun, L. Mora-Tamez and R. L. Brutchey, Design of Experiments for Nanocrystal Syntheses: A How-To Guide for Proper Implementation, *Chem. Mater.*, 2022, **34**, 9823–9835.
208 H. Zhao, W. Chen, H. Huang, Z. Sun, Z. Chen, L. Wu, B. Zhang, F. Lai, Z. Wang, M. L. Adam, C. H. Pang, P. K. Chu, Y. Lu, T. Wu, J. Jiang, Z. Yin and X.-F. Yu, A robotic platform for the synthesis of colloidal nanocrystals, *Nat. Synth.*, 2023, **2**, 505–514.
209 X. Liu, H. Yang, Y. Chen, Y. Yang, L. Porcar, A. Radulescu, S. Guldin, R. Jin, F. Stellacci and Z. Luo, Quantifying the Solution Structure of Metal Nanoclusters Using Small-Angle Neutron Scattering, *Angew. Chem., Int. Ed.*, 2022, **61**, e202209751.
210 W. You, Z. Cai, F. Xiao, J. Zhao, X. Yu, W. Wang, Z. Chen, W. Hu, G. Sun and Z. Wang, Local delivery of MoS_2/FeS_2 heterojunction by biomolecular microneedles for multimodal therapy of infected wounds, *Chem. Eng. J.*, 2024, **498**, 155722.
211 X. Ouyang, N. Jia, J. Luo, L. Li, J. Xue, H. Bu, G. Xie and Y. Wan, DNA Nanoribbon-Assisted Intracellular Biosynthesis of Fluorescent Gold Nanoclusters for Cancer Cell Imaging, *JACS Au*, 2023, **3**, 2566–2577.
212 Y. Wang, K. Huang, T. Wang, L. Liu, F. Yu, W. Sun, W. Yao, H. Xiong, X. Liu, H. Jiang and X. Wang, Nanosensors Monitor Intracellular GSH Depletion: GSH Triggers Cu(II) for Tumor Imaging and Inhibition, *Small*, 2024, **20**, 2310300.
213 S. Cestellos-Blanco, H. Zhang, J. M. Kim, Y.-x. Shen and P. Yang, Photosynthetic semiconductor biohybrids for solar-driven biocatalysis, *Nat. Catal.*, 2020, **3**, 245–255.
214 R. Burke, S. Chakraborty, K. P. McClelland, J. Jelušić, E. M. Matson, K. L. Bren and T. D. Krauss, Light-driven hydrogen production with CdSe quantum dots and a cobalt glutathione catalyst, *Chem. Commun.*, 2021, **57**, 2053–2056.
215 Z.-Q. Wei, S. Hou, X. Lin, S. Xu, X.-C. Dai, Y.-H. Li, J.-Y. Li, F.-X. Xiao and Y.-J. Xu, Unexpected Boosted Solar Water Oxidation by Nonconjugated Polymer-Mediated Tandem Charge Transfer, *J. Am. Chem. Soc.*, 2020, **142**, 21899–21912.
216 H. Liang, B.-J. Liu, B. Tang, S.-C. Zhu, S. Li, X.-Z. Ge, J.-L. Li, J.-R. Zhu and F.-X. Xiao, Atomically Precise Metal Nanocluster-Mediated Photocatalysis, *ACS Catal.*, 2022, **12**, 4216–4226.
217 X. Xiao, P.-H. Li, L. Tang, D. Wu, H. Xia, Z.-Y. Song, Y.-H. Zhao, B. Liang, M. Yang, R. Tang, J. Yao, X.-J. Huang, X. Chen and Z. Lei, Stepwise Coordination Engineering of Pt_1/Au_{25} Dual Catalytic Sites with Enhanced Electrochemical Activity and Stability, *Adv. Mater.*, 2025, 2417900.
218 R. Jin, G. Li, S. Sharma, Y. Li and X. Du, Toward Active-Site Tailoring in Heterogeneous Catalysis by Atomically Precise Metal Nanoclusters with Crystallographic Structures, *Chem. Rev.*, 2021, **121**, 567–648.
219 W. Wang, T. Wang, S. Chen, Y. Lv, L. Salmon, B. Espuche, S. Moya, O. Morozova, Y. Yun, D. Di Silvio, N. Daro, M. Berlande, P. Hapiot, J.-L. Pozzo, H. Yu, J.-R. Hamon and D. Astruc, Cu(I)-Glutathione Assembly Supported on ZIF-8 as Robust and Efficient Catalyst for Mild CO_2 Conversions, *Angew. Chem., Int. Ed.*, 2024, **63**, e202407430.
220 L. Xu, J. Chen, Q. Ma, D. Chao, X. Zhu, L. Liu, J. Wang, Y. Fang and S. Dong, Critical evaluation of the glucose oxidase-like activity of gold nanoparticles stabilized by different polymers, *Nano Res.*, 2023, **16**, 4758–4766.
221 J. Fan, X. Zhang, W. Tan, Z. Feng and K. Li, Bioinspired Surface Ligand Engineering Regulates Electron Transfers in Gold Clusterzymes to Enhance the Catalytic Activity for Improving Sensing Performance, *Nano Lett.*, 2024, **24**, 7800–7808.
222 H. Shan, J. Shi, T. Chen, Y. Cao, Q. Yao, H. An, Z. Yang, Z. Wu, Z. Jiang and J. Xie, Modulating Catalytic Activity and Stability of Atomically Precise Gold Nanoclusters as Peroxidase Mimics via Ligand Engineering, *ACS Nano*, 2023, **17**, 2368–2377.